ACS APPLIED NANO MATERIALS

www.acsanm.org Article

Hybrid Cellulose Nanocrystal-Bonded Carbon Nanotubes/Carbon Fiber Polymer Composites for Structural Applications

Shadi Shariatnia, Annuatha V. Kumar, Ozge Kaynan, and Amir Asadi*

Cite This: https://dx.doi.org/10.1021/acsanm.0c00785 Read Online

ABSTRACT: Integrating carbon nanotubes (CNTs) in carbon-fiber-reinforced-polymer (CFRP) composites enhances structural and functional properties; however, it often involves chemical functionalization or processes that lead to inhomogeneous dispersion and nonuniform distribution of CNTs that impair the final properties and hinder manufacturing scalability. Herein, we present a novel and scalable processing technique to integrate pristine CNTs (pCNTs) into CFRP composites without the need for chemical functionalization or addition of surfactants. We use cellulose nanocrystals (CNCs) as assisting nanomaterials to uniformly disperse and stabilize pCNTs in water, and then we coat carbon fibers (CFs) with CNC-pCNT prior to resin infusion. Two coating methods are used: simple immersion (I-coating) and simultaneous immersion and sonication (IS-coating). The surface chemistry of coated CFs reveals that I-coating provides a higher quantity of polar oxygen groups in coated CFs containing CNC-pCNT compared to IS-coating. We show that fabricating hybrid CFRPs by incorporating 0.2 wt % CNC−0.2 wt % pCNT in CFRP composites using this simple technique enhances the flexural strength by 33% and the interlaminar shear strength (ILSS) by 35% compared to those of neat CFRPs. Significantly, 0.2CNC-0.2pCNT-CFRPs show ∼25% higher flexural strength and ILSS compared to the largest enhancement in composites with individual functionalized CNTs (fCNTs) or CNCs, demonstrating a synergistic effect of CNC-pCNT in enhancing properties. Moreover, our results indicate that incorporating CNC-pCNT increases the thermal stability of CFs compared to those of fCNTs. These are specifically crucial in composites used in structural applications. These results highlight that the introduced CNC-enabled processing technique is a potential scalable path toward the fabrication of hybrid composites that can enhance properties higher than individual CNTs or CNCs, avoiding costly and/or time-inefficient functionalization processes.

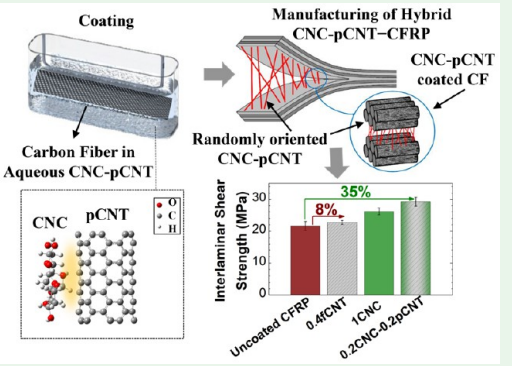

KEYWORDS: *polymer composites, carbon nanotube, cellulose nanocrystal, processing, enhanced properties*

1. INTRODUCTION

Carbon-fiber-reinforced-polymer (CFRP) composites have reached a plateau in their performance because carbon fibers (CFs) cannot reach beyond 30% of their theoretical values, and delamination has remained a major threat to composite life.[1] Theoretical and experimental studies suggest that integrating nanomaterials in CFRP composites can overcome these limitations because they transfer their outstanding properties to the composite. Owing to their superior mechanical and functional properties, carbon nanotubes (CNTs) have been applied in CFRP composites as fillers in resin matrixes or as a coating on fibers to improve the strength,[2] interfacial properties,[3−5] interlaminar strength,[6−8] electrical and thermal conductivities,[9−11] damage tolerance, and fatigue behavior.[12,13] The main routes to dispersing CNTs in polymer composites have remained unchanged for almost a decade, i.e., (i) interlayering/interleaving, where a thin layer of CNT/polymer is integrated in the midplane of the laminate,[14,15] (ii) dispersing a CNT in polymer by chemical functionalization, the addition of surfactants, or polymer wrapping,[16−19] (iii) attaching CNT directly to the CF that includes functionalization and/or charging of the surface of nanoparticles,[20−23] or wrapping of CNT into the CF,[24] (iv) electrophoresis,[12,19,25−30] (v) chemical vapor deposition (CVD),[3,31] and (vi) coating by grafting, spraying, or immersing.[32−40] Although extensive effort has been spent on processing techniques to integrate CNTs in polymer composites, these techniques often involve time/cost-inefficient processes and face a number of hurdles such as inhomogeneous dispersion of CNTs,[41] weak interfacial bonding across fiber/CNT/polymer,[42] damage on the sidewalls of CNTs that impair their intrinsic properties,[43−46] and nonscalability.

Received: March 22, 2020
Accepted: May 14, 2020
Published: May 14, 2020

Alternative nanoparticles that have high potential for increasing the properties of polymer composites are cellulose nanomaterials (CNs). CNs are generally grouped based on the cellulose source and extraction methods, leading to various CN types, including cellulose nanocrystals (CNCs), cellulose nanofibrils, algae cellulose, and bacterial cellulose. CNCs are cellulose-based (linear-chain glucose units, $C_6H_{10}O_5$, extracted mainly from trees and plants by acid hydrolysis), spindle-shaped nanoparticles (3−20 nm in width and 50−500 nm in length) with high mechanical properties (~5 GPa strength, ~150 GPa modulus, and stability of up to 300 °C), low density (1.5 g/cm^3), high aspect ratios (10−100), accessible hydroxyl side groups (−OH), and low toxicity.[47] Similar to CNTs, obtaining a good CNC dispersion in polymer systems is challenging.[48,49]

There are studies showing that using binary nanomaterials in polymers, e.g., graphene nanoplatelets (GNPs) and CNs,[50−54] CNTs and zirconium phosphate,[55,56] CNTs/GNPs and nanoclay,[57] and GNPs and cellulose nanofibers, can enhance the properties compared to systems containing a single nanomaterial.[58] In addition, there are scattered reports on using assisting nanomaterials to better disperse CNTs in polymer systems such as exfoliated zirconium phosphate nanoplatelets,[59,60] and zirconium oxide[9] and attaching metallic particles to the CNT surface;[61−63] however, the final properties of these composites did not improve compared to the polymer systems containing only functionalized CNTs (fCNTs). A few reports are also available on using CNCs to disperse graphene and CNTs in water without further using them in composites.[64−72]

In this study, we aim to develop a scalable process to accelerate the manufacturing of hybrid composites with enhanced properties suitable for structural applications. We introduce a novel processing−manufacturing method to produce hybrid (micro/nano) composites, in which we utilize CNCs as assisting nanomaterials to integrate pristine CNTs (pCNTs) into CFRPs without the need for chemical functionalization or the addition of surfactants. CNCs are used to disperse and stabilize pCNTs in water to provide the coating suspension for CFs prior to resin infusion via vacuum-assisted resin-transfer molding (VaRTM). We show that the presence of a hybrid nanomaterial system, i.e., CNC-pCNT, enhances the flexural and interlaminar properties as well as thermal stability higher than composites containing only CNC or fCNTs. These results highlight the role of CNCs in process scalability and synergistic improvement of the final properties of hybrid composites.

2. EXPERIMENTAL SECTION

2.1. Design of the Experiments. Avoiding time- and cost-inefficient functionalization steps for both CNCs and CNTs and finding the optimum nanoparticle concentration and ratio promote the scalability, reduction in materials usage, and economic viability of a CNC-assisted processing technique. As a result, it is important to compare the properties of hybrid composites containing individual CNCs and fCNTs, and combinations of CNC-pCNT with different concentrations and ratios. It is noted that individual pCNTs are not used in our experiments because it is not feasible to disperse pCNTs in water without grafting chemical groups or using dispersants. Instead, fCNTs are used because they are the mainstream CNTs integrated in polymer composites due to their stability in solvents and compatibility with most polymer systems. We used only acid-treated fCNTs in this study for simplicity.

Table S1 shows different ratios of CNC to pCNT tested for stability in water as well as the selected ratio as the appropriate recipe for coating the CFs. Section 3.1 discusses the ζ-potential and dynamic light scattering (DLS) data that led to this selection. Table 1 presents all of the coating suspensions with different concentrations used for coating, as well as the fabricated hybrid CFRP composites. We used two coating methods: simple immersion (I-coating) and simultaneous immersion and bath sonication (IS-coating). Initially, we prepared all coated CFs through I-coating. Then, those nanomaterial concentrations that resulted in the highest properties in the produced composites were selected for IS-coating to compare the effect of the coating method in enhancing properties.

Table 1. List of Manufactured Composites

coating nanomaterial	concentration (wt %)	coating technique	naming scheme of the manufactured CFRP composite
none	N/A	N/A	uncoated CFRP
CNC	0.2	(1) immersion (I-coating); (2) immersion and bath sonication (IS-coating)	0.2CNC-CFRP
	0.5		0.5CNC-CFRP
	1		1CNC-CFRP
			1CNC-IS-CFRP
	1.5		1.5CNC-CFRP
fCNT	0.01		0.01fCNT-CFRP
	0.05		0.05fCNT-CFRP
	0.2		0.2fCNT-CFRP
			0.2fCNT-IS-CFRP
	0.4		0.4fCNT-CFRP
	0.5		0.5fCNT-CFRP
CNC-pCNT	0.2−0.2		0.2CNC-0.2pCNT-CFRP
			0.2CNC-0.2pCNT-IS-CFRP
	0.5−0.5		0.5CNC-0.5pCNT-CFRP

The preparation of coating suspensions, coating process, and manufacturing of hybrid composites are discussed in sections 2.3.1, 2.3.2, and 2.3.3, respectively. The corresponding labeling scheme used to describe the coated CFs and hybrid composites is *l*CNC, *m*fCNT, and *n*CNC-*s*pCNT. *l*, *m*, *n*, and *s* represent the concentration of nanomaterials in the coating suspension. Composites prepared via IS-coating include IS in their labels.

2.2. Materials. The CF used in this work is plain woven, with a tow size of 3K (U.S. Composites Inc., West Palm Beach, FL). The resin is a bicomponent epoxy resin consisting of diglycidyl ether of Bisphenol A (635 thin epoxy) and 556 slow polyamide hardener (U.S. Composites Inc., West Palm Beach, FL). The CNCs are NCV-100 (CelluForce, Windsor, Quebec, Canada) with diameters of 2.3−4.5 nm and lengths of 44−108 nm. The multiwalled pCNTs are NC7000 (Nanocyl, Sambreville, Belgium) produced via catalytic CVD with ~90% carbon purity, an average diameter of 9.5 nm, a length of 1.5 μm, and a number of walls of 10.

2.3. Processing−Manufacturing of Hybrid Composites. The major steps of the processing−manufacturing method of the CNC-pCNT-CFRP hybrid composites are shown in Figure 1, which includes the preparation, coating, and manufacturing, as detailed below.

2.3.1. Preparation of a Coating Suspension. Three different coating systems, i.e., CNC, fCNT, and CNC-pCNT aqueous suspensions, were prepared as follows.

CNC Aqueous Suspension. As-received CNCs with 0.2, 0.5, 1, and 1.5 wt % concentrations were dispersed in 250 mL of deionized water (DI-H_2O) using probe sonication (Qsonica Q125 equipped with a sonotrode of 6 mm) for 15 min at a frequency of 20 kHz and 75% intensity.

https://dx.doi.org/10.1021/acsanm.0c00785
ACS Appl. Nano Mater. XXXX, XXX, XXX−XXX

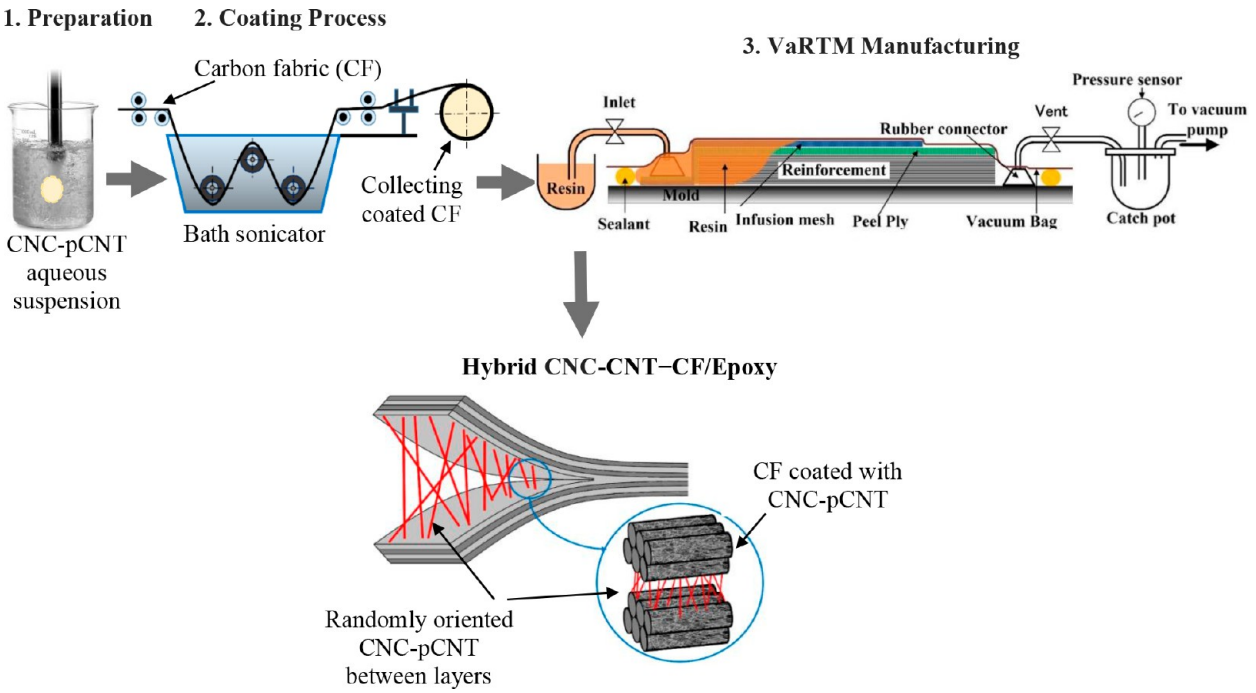

Figure 1. Processing and manufacturing of CNC-pCNT-CFRP hybrid composites: (1) Preparation of aqueous suspension of CNC-pCNT using probe sonication; (2) coating process to deposit CNC-pCNT on CF; (3) VaRTM manufacturing with coated CFs.

fCNT Aqueous Suspension. A total of 250 mg of multiwalled pCNTs was oxidized in a mixture of sulfuric and nitric acid (H_2SO_4/HNO_3 with 45/15 cubic centimeters) inside a bath sonicator (Cole-Parmer) for 2 h at 25 °C and 40 kHz. A total of 190 mL of DI-H_2O was added to the suspension, stirred in an oil bath, and sonicated for another 5 h at 60 °C. After oxidation, it was isolated with a poly(vinylidine fluoride) filter membrane under vacuum and washed four times with DI-H_2O during the filtration process to remove any trace of acid residue. fCNTs with 0.01, 0.05, 0.2, 0.4, and 0.5 wt % concentrations in water were used for coating CFs.

CNC-pCNT Aqueous Suspension. pCNTs were separately dispersed in a CNC aqueous suspension prepared according to the above procedure with various ratios and then probe-sonicated for 2 h at a frequency of 20 kHz and 75% intensity. CNC-pCNT systems with concentrations of 0.2−0.2 and 0.5−0.5 wt % were used for coating CFs.

2.3.2. Coating. Coating CFs with the prepared nanomaterials was carried out in two different methods: (i) immersion of CF in a bath filled with an aqueous suspension of CNC, fCNT, and CNC-pCNT for 15 min (I-coating); (ii) simultaneous immersion and bath sonication of CF with aqueous suspensions of CNC, fCNT, and CNC-pCNT for 5 min at 40 kHz (IS-coating). The coating duration was selected by testing different coating times (5, 10, 15, 20, and 25 min) on the control samples. Thermogravimetric analysis (TGA) data revealed that the content of nanomaterials on CF does not significantly increase after 15 min. The coated CFs were dried at room temperature for 12 h, followed by placement in an oven (Across International AT09) at 80 °C for 30 min.

2.3.3. Manufacturing. The hybrid composites were manufactured using eight coated CF layers by a VaRTM process. The CF layers were stacked and placed over a Mylar sheet on the surface of a rectangular mold. A peel ply was added on top of the CF layers to prevent sticking. Two pieces of infusion mesh were put at the top and bottom of the mold to promote resin flow. The entire package was enclosed in a vacuum bag and sealed with two-sided butyl tape. Two external hoses were connected to the inlet of the resin and vent to the vacuum pump. Prior to resin infusion, the inlet was closed, and the vacuum pump was turned on to draw out the air trapped inside the mold. After the vacuum was established, degassed resin was infused from the inlet. Excess resin was removed from the vent, the inlet was closed, and the vent was left open for 24 h until the resin was cured. Different types of samples, i.e., tensile, flexural, and short beams, were cut from the fabricated plates using a waterjet (waterjet system X-5; Jet Edge Inc., St. Michael, MN).

2.4. Characterization Techniques. *2.4.1. ζ Potential and DLS.* The ζ potential and particle size distribution of CNC, fCNT, and CNC-pCNT aqueous suspensions were measured at 25 °C using a Malvern Zetasizer Nano ZS. All of the suspensions were diluted to 0.01 wt % in DI-H_2O and stirred for 15 min at 200 rpm. The same instrument was used to measure the hydrodynamic diameters of the nanoparticles at a fixed angle of 90° at 25 °C. All experiments were carried out for at least six samples, and the average was reported.

2.4.2. X-ray Photoelectron Spectroscopy (XPS). XPS (Omicron XPS/UPS system with an Argus detector) was performed to analyze the quantitative chemical compositions on the surfaces of CNC-, fCNT-, and CNC-pCNT-coated CFs. Both I-coated and IS-coated 5 × 5 mm^2 CFs were analyzed by a monochromatic Mg Kα ($h\nu$ = 1256.6) X-ray source of 300 W operating at 15 kV. The peak analysis and quantitative elemental composition were determined by using *CasaXPS* software. All of the recorded peaks were shifted with references of 284.8 eV (C−C/C═C bond) and 532.0 eV (O═C bond) in C 1s and O 1s, respectively. Prior to XPS analysis, all of the samples were conditioned in a vacuum oven for 4 h to reduce the outgassing.

2.4.3. Transmission Electron Microscopy (TEM). A JEOL 2010 transmission electron microscope was used at 200 kV to study the morphology of CNC-pCNT with a concentration of 0.01 mg/mL. The wet samples were stained for 1 min with uranyl acetate and dried in open air.

2.4.4. Scanning Electron Microscopy (SEM). JEOL JCM-5000 (NeoCcope Tabletop) and Tescan LYRA3 scanning electron microscopes at an acceleration of 10 kV were used to study (1) the quality of the coating on the surface of CF fabrics and (2) the fracture surface of the hybrid composites. A plasma sputterer (Ted Pella Inc., Redding, CA) was used to apply gold coating on the surface of the fractured samples prior to SEM imaging to minimize charging.

2.4.5. Specific Density. A water displacement method was used to measure the specific density of the hybrid composites according to ASTM D792 to record the effect of coating on the density of the

https://dx.doi.org/10.1021/acsanm.0c00785
ACS Appl. Nano Mater. XXXX, XXX, XXX−XXX

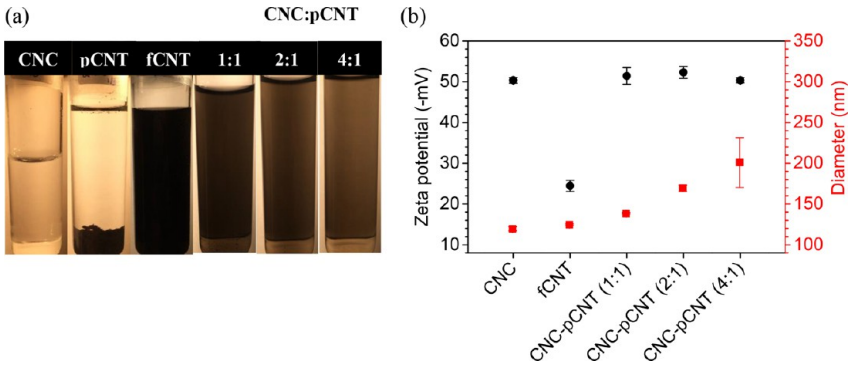

Figure 2. (a) Dispersion and stability state of the pCNT and fCNT in water with and without CNC. *n*:*m* on the vials indicates the mass ratio of CNC to CNT. (b) ζ-potential (left, black) and DLS (right, red) data of CNC-CNT suspensions in water. The concentration of each of the samples is 1 mg/mL.

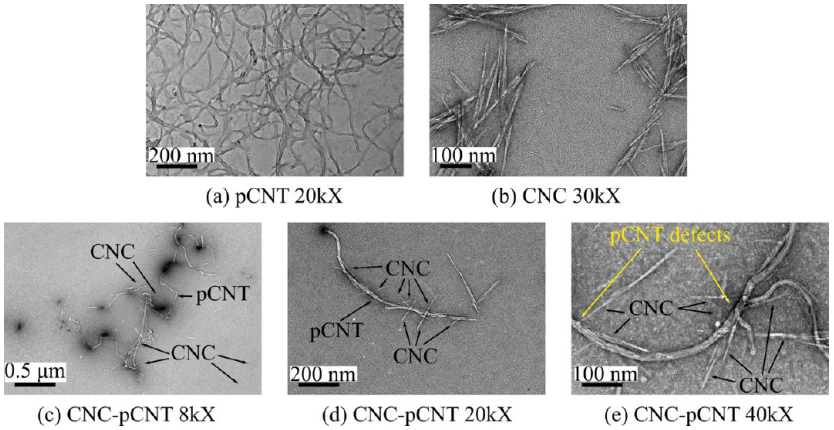

Figure 3. TEM micrographs of (a) pCNT, (b) CNC, and (c–e) CNC-pCNT.

samples. Each density data point is an average of at least 10 measurements.

2.4.6. TGA. A thermogravimetry analyzer (TA Instruments Q500) was used to determine the thermal stability of coated CFs. The samples were heated from 50 to 900 °C at 15 °C/min in an air atmosphere. Each TGA data point is an average of at least five measurements.

2.4.7. Dynamic Mechanical Analysis. A dynamic mechanical analyzer (DMA Q800; TA Instruments, New Castle, DE) in a dual cantilever mode was used to measure the effect of coating on the storage modulus, glass transition temperature (T_g), and tan δ of the samples. The temperature ramp for the test was 3 °C/min from 30 to 120 °C at a frequency of 1 Hz. A preload of 0.01 N and a maximum strain of 0.05% were applied on rectangular 60 × 13 × 2.1 mm samples. Each data point is an average of at least three measurements.

2.4.8. Mechanical Testing. The tensile properties of the hybrid composites were determined according to ASTM D638 using a Universal United STM testing system equipped with a 10 kN load cell for dog-bone samples with a gauge length of 50.8 mm, a width of 13.2 mm, and a thickness of 2.1 mm at a displacement rate of 2 mm/s. An extensometer (Instron 2630-106) with a gauge length of 25 mm was used to record the axial strain. The modulus was calculated between the axial strain values of 0.05% and 0.2%. The flexural properties were measured using a three-point bending test with the same machine according to ASTM D790 for rectangular samples with a support span of 80 mm, a width of 13.2 mm, and a thickness of 2.1 mm at a displacement rate of 2 mm/s. Short-beam-shear tests were carried out to measure the interlaminar shear strength (ILSS) of hybrid composites using an ASTM D2344 standard with a span of 25.4 and 2.1 mm thickness. Each tensile, flexural, and ILSS value is an average of at least 10 measurements.

3. RESULTS AND DISCUSSION

3.1. CNC-pCNT Dispersion and Stability in Water.

Figure 2a shows the efficacy of CNC in dispersing and stabilizing pCNT in water after 6 months. CNCs are dispersed in water because of its abundant hydroxyl (−OH) groups that form hydrogen bonds with water molecules.[73−77] Especially, CNCs treated with sulfuric acid (our case) consist of negatively charged sulfate half-ester groups that leads to colloidal stability.[78] In the absence of CNC, pCNTs will settle in a few minutes after sonication is stopped and only fCNTs remain stable in water because of the presence of hydroxyl and carboxyl groups that can make hydrogen bonds with water molecules;[79] however, their preparation requires an intensive process that might damage the CNT sidewalls because of longer exposure to an acidic environment at high temperatures and lead to low final properties in the composites.[80,81]

Figure 2b shows the ζ-potential and DLS data of CNC, fCNT, and CNC-pCNT suspensions in water with different mass ratios. The ζ-potential value for CNC-pCNT (1:1 and 2:1) is 51.5 mV, much higher than that of fCNT (25.4 mV) and on the order of that of CNCs (50.3 mV), implying the effectiveness of CNCs in dispersing pCNTs. In addition, DLS analysis shows that the average hydrodynamic diameter of CNC-pCNT (1:1) is 140 nm compared to 120 nm of CNCs and 125 nm of fCNTs. Increasing the CNC-pCNT ratio to 4:1 does not affect the ζ-potential value; however, it increases the DLS to 200 nm, implying larger aggregates. These results indicate that CNC-pCNT (1:1) is the most stable and well-

https://dx.doi.org/10.1021/acsanm.0c00785
ACS Appl. Nano Mater. XXXX, XXX, XXX−XXX

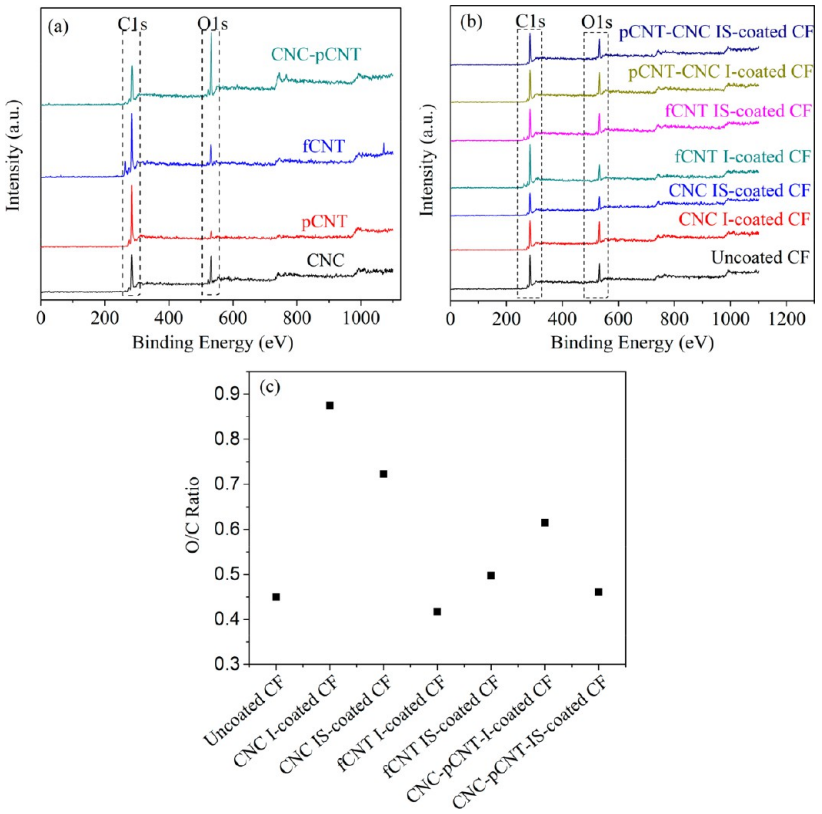

Figure 4. (a) XPS survey spectra of CNC, pCNT, fCNT, and CNC-pCNT in powder form before the coating process. (b) General view of uncoated CF, I-coated/IS-coated CNC-, fCNT-, and pCNT-CNC-CFs. (c) Atomic ratio (O/C) calculated from XPS survey spectra for coated CFs.

dispersed colloid in water; therefore, it was chosen for coating and manufacturing.

3.2. Morphology of CNC-pCNT. Figure 3 shows the TEM images of pCNT, CNC, and CNC-pCNT. The lengths of the pCNTs are in the range of a few hundred nanometers with an average diameter of 9 nm (Figure 2b), while the average length and diameter values for spindle-shaped CNCs are 150 and 8 nm, respectively (Figure 3b). CNCs tend to approach pCNTs and infiltrate them because of their smaller length scales. Although CNCs are aligned along the pCNT sidewalls, it appears that CNCs mainly tend to attach to pCNTs by their tips, as shown in Figure 3c−e, implying stronger CH−π interactions between the tip of the CNC and the sidewalls of a multiwalled CNT (MWCNT). It is noted that CNCs are more concentrated in some regions, and the higher magnification in Figure 3e suggests that these regions might be the defects on the sidewalls of pCNTs. It has also been shown in the literature that hydrophobic interactions between CNCs and the sidewalls of MWCNTs do not occur along the MWCNTs' sidewalls because of the presence of defects associated with hydrophilic groups that hinder effective hydrophobic interaction.[82,83] In contrast to MWCNTs, CNCs prefer to align along the sidewalls of single-walled CNTs (SWCNTs) because of hydrophobic interactions between the SWCNT surface and the hydrophobic (200) crystalline plane of the CNC possibly due to higher curvature.[64] The individual CNCs do not tend to agglomerate once they attach to pCNTs, suggesting that the binding between CNC and pCNT is stronger compared to that of individual CNCs. This has been further supported by XPS results in Table S2. The overall percentage of O 1s to C 1s in CNC-pCNT demonstrates a significantly higher ratio compared to CNC, fCNT, and CNC-fCNT. The higher O 1s to C 1s ratio suggests that a more active surface is available on the coated fiber for binding/bonding with epoxy, and thus better adhesion across the fiber and matrix, better stress transfer efficiency, and higher strength can be achieved. In the case of fCNT, studies have shown that although acid treatment creates chemical groups that are compatible with the polymer, leading to an improvement of interfacial adhesion, it causes damage to the sidewalls of CNTs that impairs their intrinsic properties.[41−44] Deteriorating effects of sulfonitric acid treatment on the exterior wall of CNTs have been studied and proven in the literature.[46] Also, in the TEM images, some CNTs show open ends due to the higher oxidation on the CNTs tips, which indicates C=C bond breakages. These findings imply that acid treatment results in chemical modification and morphological changes on the sidewalls of CNTs.

3.3. Surface Chemistry of Coated CFs. Figure 4a shows the overall percentage and elemental composition of various combinations of CNT, pCNT, and fCNT in the form of powder, which is also quantitatively depicted in Table S2. In the overall view, the C 1s peaks were fitted to a binding energy of 284.8 eV, whereas the O 1s peak exhibits a binding energy of 532 eV. Moreover, CNC-pCNT powder contains the highest O/C ratio with 71.32%. followed by CNC powder with 61.69%. The O/C ratio of fCNT is 26.19% compared to pCNT's ratio of 13.45%, indicating the contribution of functionalization. The high-resolution spectra of the powders can be found in Figure S1.

Figure 4b shows the survey spectra of uncoated and I- and IS-coated CFs with 1 wt % CNC, 0.4 wt % fCNT, and 0.2 wt %

https://dx.doi.org/10.1021/acsanm.0c00785
ACS Appl. Nano Mater. XXXX, XXX, XXX−XXX

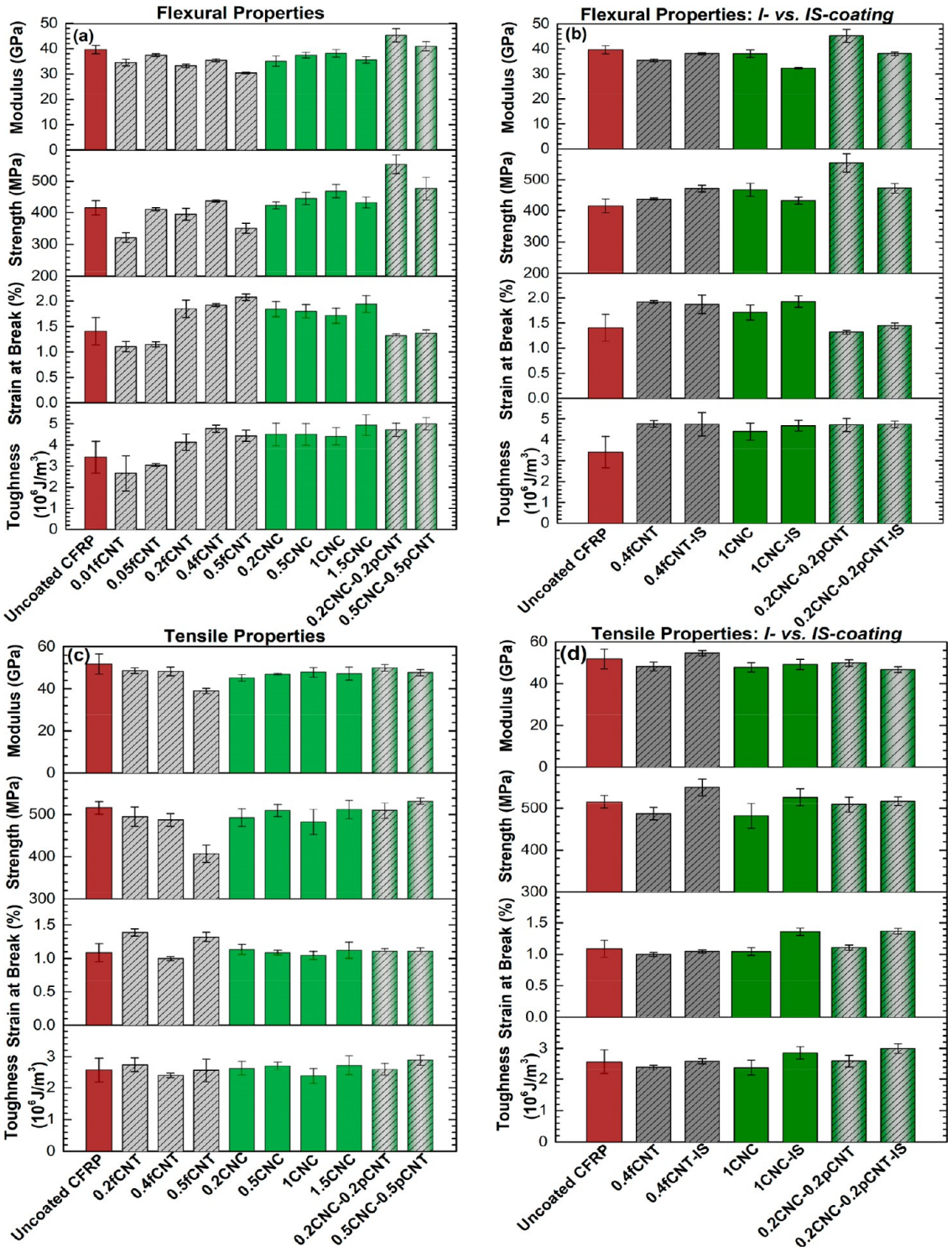

Figure 5. Effects of CNC, fCNT and CNC-pCNT in the coating suspension on: (a) flexural properties of CFRP composites with CFs coated via I-coating; (b) flexural properties of CFRP composites with CFs coated via I-coating and IS-coating; (c) tensile properties of CFRP composites with CFs coated via I-coating; (d) tensile properties of CFRP composites with CFs coated via I-coating and IS-coating.

CNC-0.2 wt % pCNT. The plots indicate that the addition of CNC I-coating and CNC-pCNTs I-coating to CFs increases the polar oxygen groups by 47% and 38%, respectively, compared to that of uncoated CFs, delineating more active surfaces for CFs and thus larger numbers of sites for strong bonding/binding with the polymer matrix.[84] Furthermore, Figure 4b and Table S2 demonstrate that a CNC-based IS-coated CF has lower oxygen on the surface compared to an I-coated CF. Figure 4c summarizes the overall atomic ratio (O/C) of coated CFs. The graph shows that there is a noticeable decrease in the O/C ratio for IS-coated CFs in CNC-based suspensions. We hypothesize that IS-coating causes CNC agglomerates or disturbs the repulsive forces of CNC colloids because of the high amount of energy or excessive heat generated through ultrasonication.

https://dx.doi.org/10.1021/acsanm.0c00785
ACS Appl. Nano Mater. XXXX, XXX, XXX−XXX

Figure S2 compares the C 1s peaks of I-coated, IS-coated, and uncoated CFs. The reference uncoated CF (Figure S2a) is primarily composed of graphite (284.8 eV) with 77.9%, polar-oxygen-containing groups including both alcohol, C−O (∼286.2 eV), and carbon in carboxyl or ester groups, C═O (∼288.8 eV), occupying approximately 22%, and finally a slight $\pi-\pi$ binding (∼290.5 eV). Parts b and c of Figure S2 show that I-coated CNC-CFs does not change the surface chemistry of CFs compared to uncoated CF; however, oxidative sites decrease in IS-coating (i.e., coating in an ultrasonic bath) where carboxyl groups completely vanish, indicating the effectiveness of the I-coating method for higher surface activity for CNC-coated CFs compared to that the IS-coating method. For the case of fCNT, this trend is reverse; i.e., the fCNT IS-coated CF surface has more polar oxygen groups compared to the fCNT I-coated CF, as shown in Figure S2d,e, which is consistent with previous reports where an ultrasonic bath provides an efficient dispersion for CNT-based solutions.[85] Also, the fractions of sp^2 (graphite) and sp^3 (diamond), which have been seen in fCNT-coated CFs, affect the materials' electronic and optical properties, so we combine them as a C−C group in this paper.[86] A comparison of parts f and g of Figure S2 reveals that the CNC-pCNT I-coated CF surface contains approximately 35% polar oxygen groups, compared to 2.23% of the CNC-pCNT IS-coated CF. In addition, the unsymmetrical-shaped plot of the CNC-pCNT I-coated CF compared to both the fCNT IS-coated CF and CNC-pCNT IS-coated CF plots implies an improvement in the number of polar oxygen groups on the surface of CF. Increasing the polar oxygen groups provides an active surface for epoxy to bond that results in enhanced interfacial and mechanical properties of the composites.[87,88]

3.4. Mechanical Properties. *3.4.1. Flexural and Tensile Properties.* Figure 5 shows the flexural properties of the hybrid composites made with CF coated with fCNT, CNC, and CNC-pCNT through two coating methods. Figure 5a shows that, compared to uncoated composites, the addition of fCNT in the range of 0.2−0.4 wt % slightly increases the strength by 5% and addition of fCNT lower than 0.2 wt % or higher than 0.4 wt % reduces the strength. The decrease in strength can be attributed to (1) the introduced damages to the CNT sidewalls because of the intense functionalization process[45,80] and (2) weak interfacial binding across the fiber and matrix due to agglomeration at higher concentration. For composites containing CNC, the addition of 1 wt % CNC enhances the strength by ∼12% compared to that of uncoated CFRP. The larger enhancement of the strength in CNC-CFRP compared to fCNT-CFRP is attributed to more effective interfacial and interlaminar adhesion within and across the layers. Furthermore, the XPS results (Figure 4) show that the CNC I-coated CF has a higher quantitative polar oxygen group (46.64% for CNC in comparison to 29.43% for fCNT) compared to that of the fCNT I-coated CF, creating stronger physical binding and covalent bonds with epoxy chemical groups and thus enhancing the adhesion across CF/CNC/epoxy and between neighboring layers. For 0.4fCNT-CFRP and 1CNC-CFRP composites, the strain at failure values are 36% and 21% and the toughness values are 40% and 32%, respectively, higher than those of uncoated CFRP. Multiple fracture mechanisms such as crack bridging in the presence of nanomaterials can increase the toughness, as discussed in the Fracture Surface Morphology section. Adding only CNC or fCNT does not significantly alter the flexural modulus compared to that of uncoated composites.

Integrating CNC-pCNT improves the flexural strength higher than those composites containing only fCNT or CNC. For CNC-pCNT, 0.2−0.2 and 0.5−0.5 wt % were selected as these concentrations to provide a direct comparison to 0.4fCNT and 1CNC containing CFRPs that exhibited the highest property enhancement. The flexural strength of 0.2CNC-0.2pCNT-CFRP composites is 33% higher than that of uncoated composites. It is noted that this enhancement is 20% and 30% higher than the maximum improvement in strength by CNC and fCNT, respectively. Because the flexural properties are a combination of in-plane and out-of-plane properties, this enhancement reflects that the created synergy by CNC-pCNT enhances both the interfacial and interlaminar adhesion more effectively than only CNC or fCNT. In addition to the polar oxygen groups provided by CNCs as supported by the XPS results, pCNTs have also contributed to interlaminar adhesion, acting as nanopins between the adjacent layers in CNC-pCNT-coated CFRP. The combination of these effects is likely to synergistically enhance the flexural strength. It is noted that this improvement cannot be because of the higher content of nanomaterials in 0.2CNC-0.2pCNT as it is equal to 0.4fCNT-CFRP and smaller than 1CNC−CFRP, both representing the largest enhancements in their group. Moreover, in contrast to CNC and fCNT, incorporating 0.2CNC-0.2pCNT increases the modulus by 15%, suggesting that the presence of CNC-pCNT at the interface can result in an increase in the stiffness of the fiber/matrix interphase,[89] i.e., a faster rate of stress transfer across the fiber/matrix and thus a higher modulus for the composite.[90] Although this hypothesis could not be validated in this study, Gao et al. showed that increases in the apparent modulus at the GF/epoxy interphase increase the composite macroscopic modulus.[91] Another potential reason can be related to the thickness of the interface. According to the DLS results (Figure 2b), the hydrodynamic diameter of CNC-pCNT (1:1) is slightly larger than that of fCNT. Assuming similar conditions for coating, the thickness of the coating for 0.2CNC-0.2pCNT must be accordingly larger compared to that of 0.4fCNT because the amount of nanomaterials is similar. Previous reports show that increases in the thickness of the interphase up to 2 μm enhances the interfacial shear strength (IFSS) value.[42] In contrast, there are studies suggesting that reducing the thickness of the interphase increases the IFSS.[92] Although the interface strength is usually related to the tensile strength (and not the flexural strength), these studies indicate that there should be an optimum value for the thickness of the interphase that depends on the coating process, agglomeration degree, and type of nanomaterials. In our case, 0.2CNC-0.2pCNT provides the optimum value for maximum enhancement of the properties. Increasing CNC-pCNT to 0.5−0.5 wt % decreases the flexural strength, as seen in Figure 5a. The strain at break for CNC-pCNT composites is similar to that of uncoated composites, and the toughness has increased because of the increase in the strength.

The flexural properties of hybrid composites fabricated via I-coating and IS-coating are compared in Figure 5b. It should be noted that only composites with the highest properties (Figure 5a) have been selected for Figure 5b. IS-coating has enhanced the flexural strength of 0.4fCNT-CFRP composites by 8%, while it has reduced the strength of 1CNC-CFRP and 0.2CNC-0.2pCNT-CFRP composites by 8% and 17%,

https://dx.doi.org/10.1021/acsanm.0c00785
ACS Appl. Nano Mater. XXXX, XXX, XXX−XXX

respectively. These observations show that, contrary to fCNT-coated CFs, the quality of the coating is adversely affected by IS-coating when CF fabrics are coated with CNC and CNC-pCNT. In other words, IS-coating reduces the dispersion and uniformity of the distribution on CF fabrics coated with CNC and CNC-pCNT. This is consistent with the surface chemistry of the coated CFs shown in Figure 4 and Table S2, where CNC and CNC-pCNT I-coated CFs contain higher active oxygen groups than IS-coated CFs, while fCNT I-coated CFs possess lower active oxygen groups than IS-coated CFs. The plausible mechanisms can be related to the disturbance of favorable bonds of CNC with pCNT and CF due to the ultrasonication energy that will be further discussed.

As seen in Figure 5c, the addition of CNC, fCNT, and CNC-pCNT does not statistically affect the tensile properties of composites fabricated via the I-coating process. The effects of IS-coating and I-coating on the tensile properties are compared in Figure 5d. It is observed that IS-coating has improved the tensile strength of 0.2fCNT-CFRP composites by 8% compared to neat composites, but this is not statistically significant because of the overlap of the error bars. I-coating did not change the tensile strength of 0.2fCNT-CFRP composites relative to neat composites. In general, coating CFs did not drastically change the tensile properties because the CFRPs usually possess high in-plane properties without the addition of nanomaterials. Generally, coating fibers with CNTs enhance the out-of-plane properties because they act as nanopins between neighboring layers that can, in turn, retard delamination. Although delamination is a major damage mode that can lead to catastrophic failure in both tensile and flexural loading types, in flexural loading, delamination usually occurs concurrently with other damage modes such as matrix cracking and thus is more susceptible to interlayer adhesion compared to tensile loading, where delamination usually appears at the final loading stages.[93,94]

3.4.2. Interlaminar Strength. The effects of the fCNT, CNC, and CNC-pCNT contents on the interlaminar properties of the hybrid CFRP composites are plotted in Figure 6. Coating the CF layers with 1 wt % CNC or 0.2−0.5 wt % fCNT increases the ILSS by 23% and 9%, respectively, as seen in Figure 6a. The trend is similar to that of the flexural properties: There is an optimum condition for both CNC (1 wt %) and fCNT (0.5 wt %) after which the ILSS reduces, possibly due to the agglomeration of nanoparticles, leading to slipping and poor binding across the layers.[95] The hybrid CFRP composites containing CNC-pCNT show a higher ILSS value compared to those with only CNC or fCNT. Coating the CF with 0.2CNC-0.2pCNT increases the ILSS value by 35% compared to that of uncoated composites and 12% and 24% compared to those of CFRP with 1CNC and 0.2−0.5fCNT, respectively. These results demonstrate that CNC-pCNT synergistically creates a stronger interlayer adhesion across the layers compared to that of only CNC or fCNT, as discussed in flexural strength. Figure 6b compares the ILSS values of hybrid composites coated via I-coating and IS-coating methods. Despite the variations not being significant, the trend is similar to that observed in flexural properties comparing I-coating and IS-coating: in IS-coating, when CNC is present either as the sole nanoparticle or with pCNTs, the out-of-plane properties decrease by 7% in contrast to those of I-coating.

The interlaminar properties correlate with the XPS results where CNC and CNC-pCNT I-coated CFs have more active surfaces compared to IS-coated CFs as well as pCNTs acting as

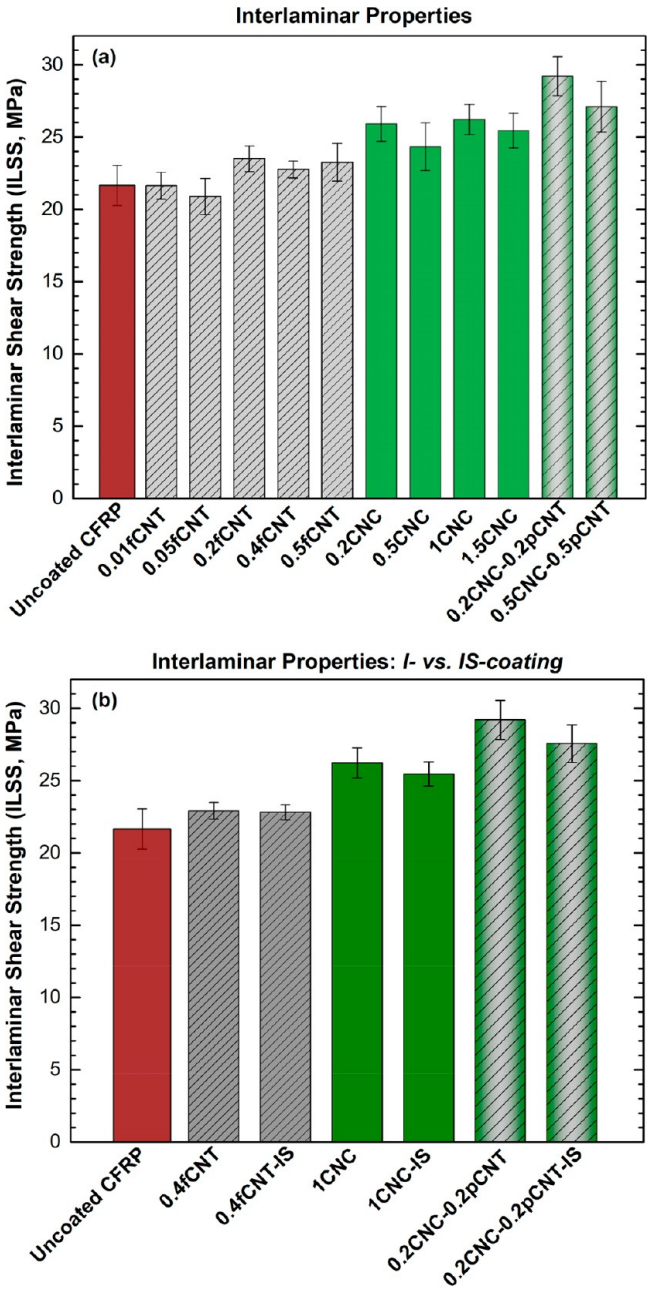

Figure 6. Effects of CNC, fCNT, and CNC-pCNT in the coating suspension on: (a) ILSS of CFRP composites with CFs coated via I-coating; (b) ILSS of CFRP composites with CFs coated via I-coating and IS-coating.

nanopins between the layers, resulting in a better interlaminar performance.[96]

3.5. Quality of the Coating. Figure 7 shows the SEM micrographs of the CFs coated with CNC, fCNT, and CNC-pCNT with I-coating and IS-coating. Interestingly, the quality of the coating depends on both the type of nanoparticle and the method of coating. When CNC is used in the coating suspension, either as the sole nanomaterial or in company with pCNT (CNC-pCNT), the IS-coating deteriorates the quality of the coating and results in the formation of scattered agglomerates on the surface of the CF, as shown in parts b,c and d,e of Figure 7, respectively, which can further negatively affect the strength of the produced composites by reducing the adhesion across the fiber/matrix and between adjacent layers

https://dx.doi.org/10.1021/acsanm.0c00785
ACS Appl. Nano Mater. XXXX, XXX, XXX−XXX

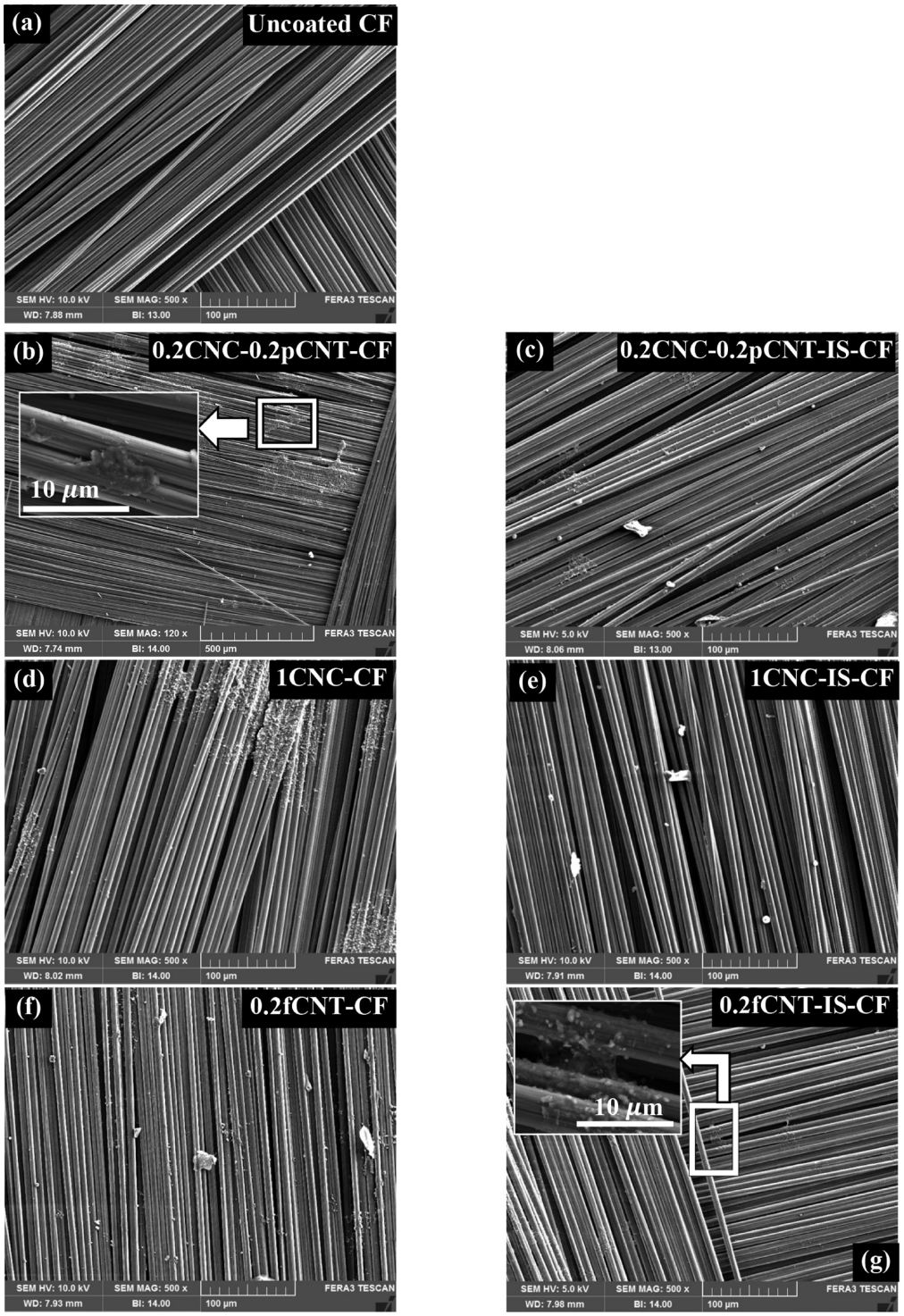

Figure 7. SEM images of (a) uncoated CF, (b) 0.2CNC-0.2pCNT-CF, (c) 0.2CNC-0.2pCNT-IS-CF, (d) 1CNC-CF, (e) 1CNC-IS-CF, (f) 0.2fCNT-CF, and (g) 0.2fCNT-IS-CF. The scale bars are 100 μm.

of composites, as depicted in the flexural and ILSS properties in Figures 5b and 6b. This is also consistent with the XPS results, where the CNC I-coated CF has more polar oxygen groups than the CNC-IS coated CF (Figures 4 and S2 and Table S2), indicating that in the I-coating a better state of dispersion and a more uniform and broader distribution are achieved compared to those in IS-coating. For fCNT, the IS-coating exhibits a better dispersion and a more uniform distribution of nanoparticles, as shown in Figure 7e,f, reflected in higher flexural, tensile, and interlaminar properties compared to those of the I-coating, as shown in Figures 5b,d and 6b. This has been also confirmed by the XPS results in Figure S2, in which fCNT IS-coated CFs have approximately 3 times higher carboxyl groups compared to I-coated CFs in high-resolution C 1s spectra. It is worth noting that, although the optimum ratio of CNC to CNT has been measured to create hybrid nanomaterial systems with maximum possible distance and minimum possible size, the formation of

https://dx.doi.org/10.1021/acsanm.0c00785
ACS Appl. Nano Mater. XXXX, XXX, XXX−XXX

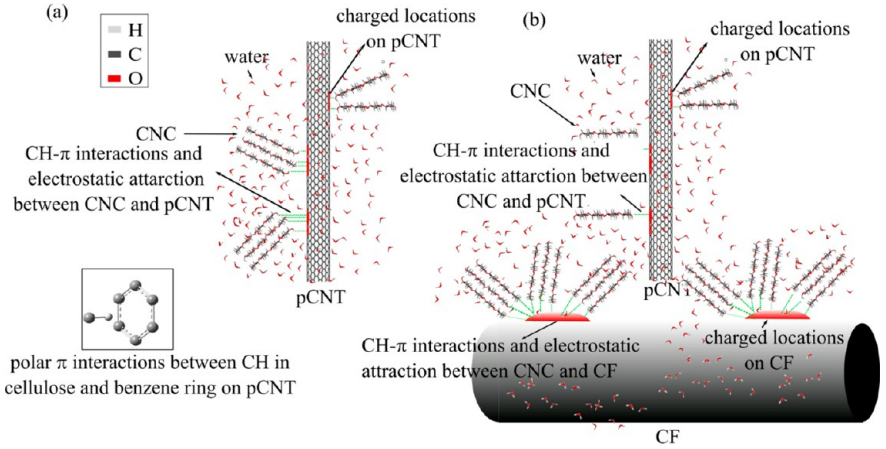

Figure 8. Schematic of interactions (a) between CNC and pCNT in water and (b) among CNC, pCNT, and CF in water during IS-coating.

aggregates is inevitable because the coating bath volume and nanomaterial concentrations have not been optimized. Overall, concurrent sonication and immersion provides better dispersion and distribution state for fCNTs but deteriorates the dispersion and uniform distribution on the CFs when CNCs are present in the coating suspension. A plausible explanation can be inherent in the binding mechanism between CNC and pCNT.

Because pCNTs contain no grafted chemical groups and the number of defects will possibly be equal on pCNT and fCNT, the binding mechanisms between CNC and pCNT are (1) polar−π interactions between the CH group in cellulose and the carbon rings of pCNT and (2) electrostatic attraction specifically in water due to fluctuation of the counterions on CNCs that further interact with the carbon atoms and induce local charges on the surface of pCNTs, as shown in Figure 8a.[72] When CNCs are present, they disperse and stabilize pCNTs in water. As CFs are introduced to the IS-coating process, it is plausible that sonication disengages the polar−π interactions and disrupts the favorable electrostatic attraction between CNC and pCNT. The disengaged CNCs tend to approach the CF, on which there are abundant carbon rings and defects for interactions compared to those of pCNTs, as illustrated in Figure 8b. In addition, the migrations of CNCs toward CF induce electrostatic charges similar to the mechanism explained for pCNT. Because these locations vary throughout the CF fabric, the CNC concentration will vary within the CF fabric, resulting in agglomeration and inhomogeneous distribution of CNCs and CNC-pCNTs onto the CF and thus lower mechanical properties compared to those of I-coating.

3.6. Thermomechanical Properties. The thermomechanical properties including the glass transition temperature (T_g), tan δ, and storage moduli below and above T_g (elastic response to energy absorption) of the CFRPs coated with CNC, fCNT, and CNC-pCNT with various contents are presented in Table S3. At 25 °C below T_g, the storage moduli of the 0.2CNC-0.2pCNT-CFRP and 0.2fCNT-IS-CFRP composites are in the range of neat composites delineating that, for CNC-pCNT-containing composites, I-coating is more efficient and, for fCNT containing composites, IS-coating is a better method in yielding higher storage moduli at the glassy state region. IS-coating has decreased the storage modulus of 0.2CNC-0.2pCNT-IS-CFRP by ∼20% compared to that of neat CFRP, indicating that the sonication energy interrupts the created bonds between CNC and pCNT, creating agglomerates and possibly preventing energy-favorable interactions between oxygen-containing functional groups of CNCs and CF/epoxy matrix. Above T_g, almost all of the composites show similar storage moduli, which is expected because the nanoparticles exist on the surface of fibers and cannot restrain the chain segmental motion. Integrating the nanomaterials does not affect T_g and tan δ of hybrid composites.

3.7. Fracture Surface Morphology. Figure 9 shows the SEM images of the fractured surfaces failed under a short beam test for the hybrid composites. Coating the CFs via I-coating and IS-coating has different effects on the morphology. Compared to neat CFRPs, composites coated with CNC-pCNT or CNC via I-coating exhibit a rigged fracture surface with shear cusps and shorter broken fibers, as shown in Figure 9b,d. A similar morphology is observed for fCNT-CFRP prepared via IS-coating, as shown in Figure 9g. In addition, these images show that the presence of nanoparticles suppresses crack propagation at different locations and deviates its path, suggesting that matrix crack propagation has been delayed and converted to a tortoise path compared to a straight matrix crack in neat CFRPs shown in Figure 9a. These mechanisms can increase the strength of the composites, as indicated in Figures 5a,b and 6a,b. In contrast, when CNC and CNC-pCNT are used in IS-coating (Figure 9c,e) or fCNT is used in I-coating (Figure 9f), the fracture surface morphology is altered: the cracks propagate through the depth and breadth of the sample, the number of shear cusps and plastically deformed areas of the matrix decrease, the number and length of debonded fibers devoid of a matrix increase, and sharp edges increase. These observations suggest that the adhesion between the fiber and matrix is weaker in IS-coated CNC and CNC-pCNT and I-coated fCNT composites, which ultimately affects the final strength. These schemes are consistent with the quality of the dispersion and uniformity of the distribution (Figure 7), ILSS values (Figure 6), and XPS results (Figure 4).

Figure 10 shows the SEM images of fractured surfaces that failed in tensile tests. Although the tensile properties of coated composites did not differ from those of uncoated composites, the fracture morphology can reveal information on enacting failure mechanisms. The general trend is similar to that of the fractography results in Figure 9 and consistent with the coating quality in Figure 7. In composites coated with CNC and CNC-pCNT through I-coating, the matrix surfaces are rougher

https://dx.doi.org/10.1021/acsanm.0c00785
ACS Appl. Nano Mater. XXXX, XXX, XXX−XXX

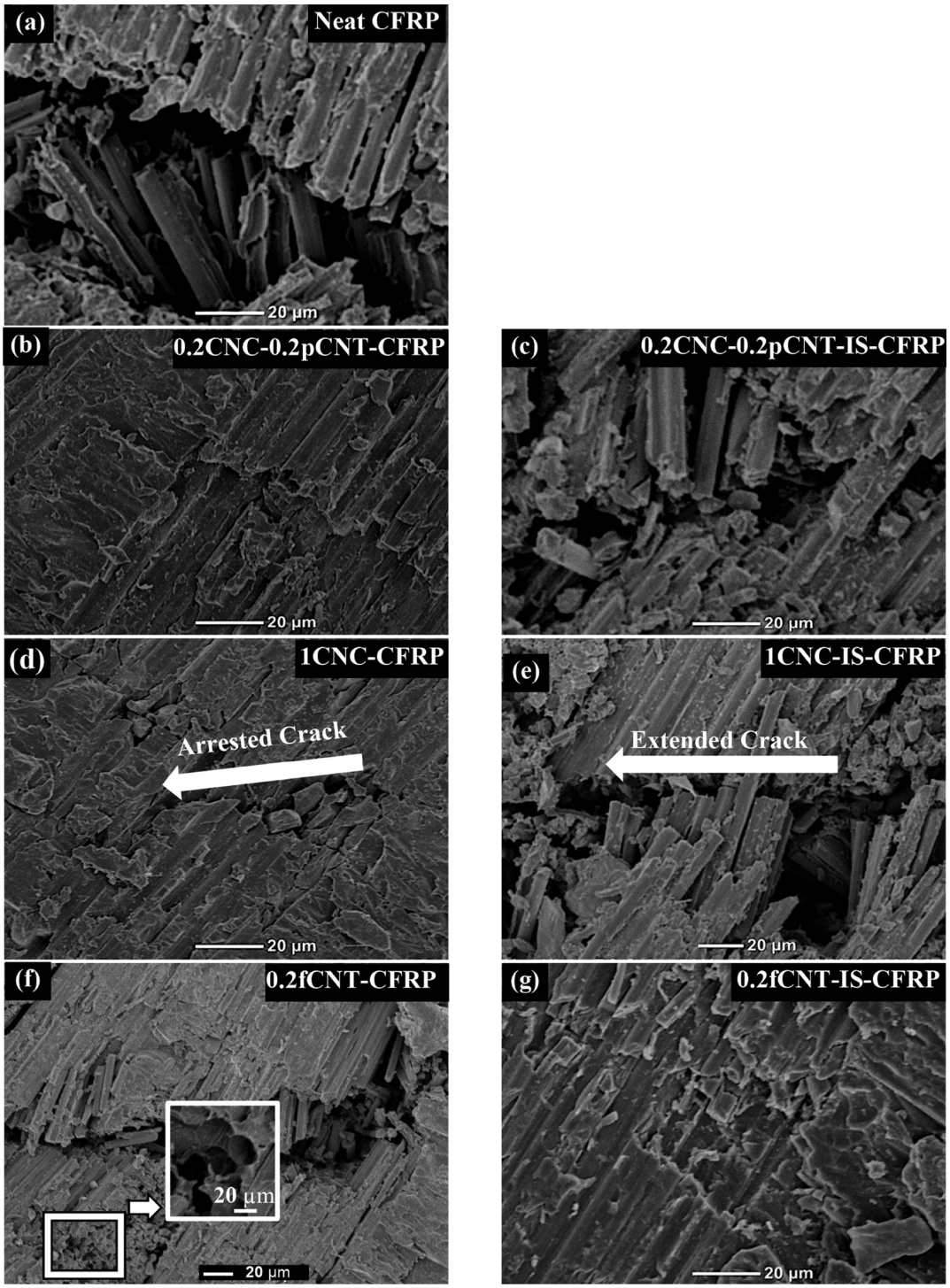

Figure 9. SEM images of fractured surfaces of samples that failed in short beam tests: (a) neat CFRP; (b) 0.2CNC-0.2pCNT-CFRP; (c) 0.2CNC-0.2pCNT-IS-CFRP; (d) 1CNC-CFRP; (e) 1CNC-IS-CFRP; (f) 0.2fCNT-CFRP; (g) 0.2fCNT-IS-CFRP. The scale bars are 20 μm.

compared to those in composites prepared via IS-coating (Figure 10b,d), where more pulled-out/detached fibers often devoid of a matrix exist (Figure 10c,e). These mechanisms suggest that I-coating provides better adhesion across the fiber and matrix for CNC-containing composites. However, for composites containing fCNT, this trend is reversed; i.e., IS-coating results in rougher fracture surfaces, shear cusps, and plastic deformation (Figure 10g), suggesting higher energy absorption before failure compared to that of I-coating (Figure 10f).

3.8. Thermal Stability and Specific Density. The density for all composites is 1.45 ± 0.03 g/cm^3 independent of the coating materials and coating method, indicating that the presence of CNC and/or CNT on the CF did not alter the resin infusion or add weight to the produced composites.

Figure 11 reports the TGA and differential thermogravimetry (DTG) curves obtained from TGA of CFs coated with CNC, fCNT, and CNC-pCNT using both coating techniques of I-coating and IS-coating. The TGA and DTG curves are superimposed to facilitate analysis.

https://dx.doi.org/10.1021/acsanm.0c00785
ACS Appl. Nano Mater. XXXX, XXX, XXX−XXX

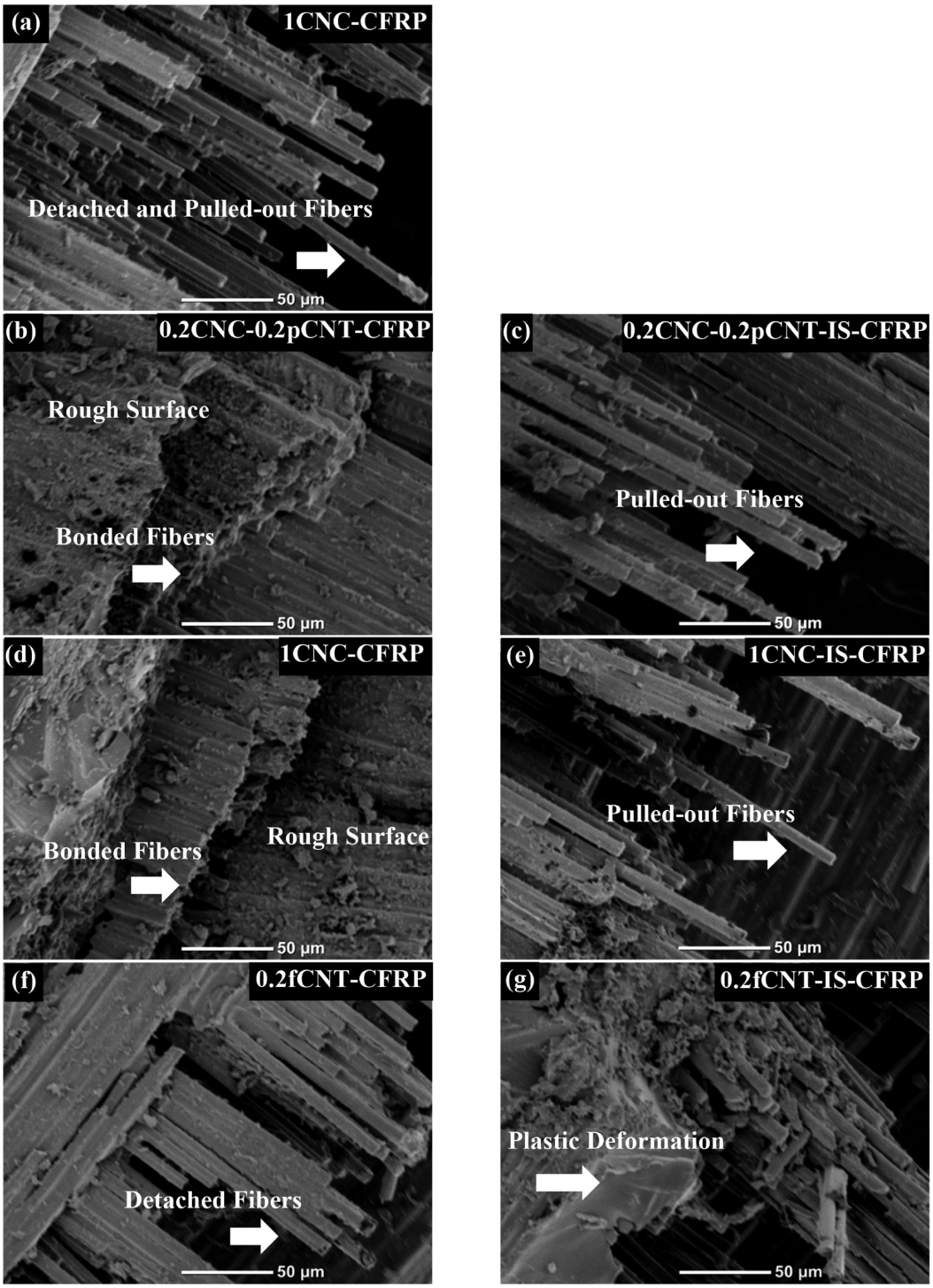

Figure 10. SEM images of fractured surfaces of samples that failed in tensile tests: (a) neat CFRP; (b) 0.2CNC-0.2pCNT-CFRP; (c) 0.2CNC-0.2pCNT-IS-CFRP; (d) 1CNC-CFRP; (e) 1CNC-IS-CFRP; (f) 0.2fCNT-CFRP; (g) 0.2fCNT-IS-CFRP. The scale bars are 50 μm.

To study the thermal stability of coated CFs, those that resulted in the highest mechanical properties were selected. The onset of degradation and decomposition temperatures of uncoated CFs are 790 and 900 °C, respectively. The onset of degradation temperature for both 0.2fCNT-CF and 0.2fCNT-IS-CF is ~750 °C, which is lower than those of CNC-CF (810 °C) and CNC-pCNT-CF (830 °C). For fCNT-IS-CF, the onset temperature is slightly higher than that of fCNT-CF by 10 °C, indicating that simultaneous sonication and immersion during coating has increased the thermal stability of fCNT-coated CFs because of the better dispersion and distribution state, as previously discussed. Compared to uncoated CFs, adding fCNT lowers the thermal stability of the fibers by reducing the onset temperature from 790 to 750 °C and accelerates the rate of decomposition because fCNT-CF reaches a plateau at 800 °C compared to 900 °C of uncoated CFs. The decrease in the thermal stability is a major concern in aerospace composites. Despite the contradictory results in the literature on the effect of CNT on the improvement or deterioration of the thermal stability of composites containing

https://dx.doi.org/10.1021/acsanm.0c00785
ACS Appl. Nano Mater. XXXX, XXX, XXX−XXX

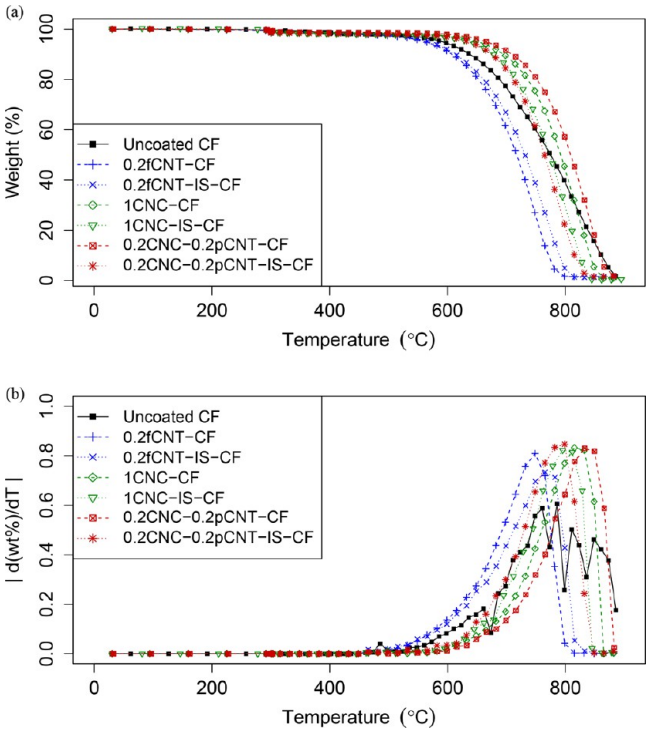

Figure 11. (a) TGA and (b) DTG curves.

CNTs,[97−101] it has been shown that the type of metal catalysts on CNTs can accelerate or decelerate thermal degradation.[100] In our study where the metal catalysts are aluminum and cobalt, thermal degradation of fCNT-CFs is accelerated,[100] as shown in Figure 11.

When CFs are coated with 1 wt % CNC and 0.2CNC-0.2pCNT, the onset temperature increases to 810 and 830 °C, respectively, compared to 790 °C of uncoated CFs. Specifically, for 0.2CNC-0.2pCNT, the coated CFs reach a plateau at 900 °C similer to that of uncoated CFs, highlighting that the combination of CNC-pCNT increases the thermal stability of CFs. Although both CNC and pCNT start to degrade at lower temperatures (300 and 600 °C, respectively) than that of neat CFs (790 °C), a very low thermal conductivity of CNCs (~5.7 W/mK[47]) seems to delay the transitioning of heat to CFs and thus retards the decomposition process. When IS-coating is applied, the onset temperature decreases for CNC- and 0.2CNC-0.2pCNT-IS-coated CFs, which is consistent with the discussion on the effect of bath sonication on the formation of agglomerates on the CFs and thus the uneven distribution of nanoparticles that can accelerate thermal decomposition.

4. CONCLUSION

In this study, we used CNCs to disperse and stabilize pCNTs in water to coat CFs prior to manufacturing hybrid CFRPs without the need for time/cost-inefficient chemical functionalization. Two coating methods, i.e. immersion (I-coating) and simultaneous immersion and bath sonication (IS-coating), were examined. Our results show that I-coating is more effective in dispersing and uniformly depositing CNC and CNC-pCNT, whereas IS-coating is a better technique for depositing fCNT onto the CFs. Adding CNC-pCNT by I-coating increased the flexural modulus and strength of hybrid CFRPs by 15% and 33% and ILSS by 35% compared to those of neat composites. In particular, CNC-pCNT-CFRP composites exhibited ~25% higher flexural strength and ILSS compared to the highest values of CFRPs containing fCNT. The combined effect of CNC in increasing polar oxygen groups on the surface of CFs and pCNTs acting as nanopins results in better adhesion across the fiber and matrix and between neighboring layers, leading to synergistic enhancement of the flexural and interlaminar strength. Moreover, adding CNC-pCNT increased the onset temperature of thermal degradation of CF by 40 °C, in contrast to a 40 °C decrease in the onset temperature of CF when fCNT was added. These results indicate that the introduced CNC-assisted processing technique is effective in manufacturing of hybrid CNT-CFRP composites with enhanced properties and thermal stability, highlighting a path forward in scalable processing of hybrid composites for structural applications.

■ ASSOCIATED CONTENT

Supporting Information

The Supporting Information is available free of charge at https://pubs.acs.org/doi/10.1021/acsanm.0c00785.

Optimum nanomaterial mass-ratio selection, XPS analysis results for various powder and coated CFs, high-resolution C 1s peaks of uncoated, I-coated, and IS-coated CFs, and effect of CNC, fCNT, and CNC-pCNT on the viscoelastic properties of hybrid CFRP composites (PDF)

■ AUTHOR INFORMATION

Corresponding Author

Amir Asadi − *Manufacturing and Mechanical Engineering Technology, Department of Engineering Technology and Industrial Distribution, Department of Materials Science and Engineering, and J. Mike Walker '66 Department of Mechanical Engineering, Texas A&M University, College Station, Texas 77843, United States;* orcid.org/0000-0002-3174-362X; Phone: +1 (979)-458-7841; Email: amir.asadi@tamu.edu

Authors

Shadi Shariatnia − *J. Mike Walker '66 Department of Mechanical Engineering, Texas A&M University, College Station, Texas 77843, United States*

Annuatha V. Kumar − *J. Mike Walker '66 Department of Mechanical Engineering, Texas A&M University, College Station, Texas 77843, United States*

Ozge Kaynan − *Department of Materials Science and Engineering, Texas A&M University, College Station, Texas 77843, United States*

Complete contact information is available at: https://pubs.acs.org/10.1021/acsanm.0c00785

Notes

The authors declare no competing financial interest.

■ ACKNOWLEDGMENTS

The authors thank Minh Tran and Mohammad Aramfard for their contributions in conducting experiments. This material is based upon work supported by the National Science Foundation under Grant 1930277.

https://dx.doi.org/10.1021/acsanm.0c00785
ACS Appl. Nano Mater. XXXX, XXX, XXX−XXX

REFERENCES

(1) Chae, H. G.; Newcomb, B. A.; Gulgunje, P. V.; Liu, Y.; Gupta, K. K.; Kamath, M. G.; Lyons, K. M.; Ghoshal, S.; Pramanik, C.; Giannuzzi, L.; Şahin, K.; Chasiotis, I.; Kumar, S. High strength and high modulus carbon fibers. *Carbon* **2015**, *93*, 81−87.

(2) Zhou, H. W.; Mishnaevsky, L.; Yi, H. Y.; Liu, Y. Q.; Hu, X.; Warrier, A.; Dai, G. M. Carbon fiber/carbon nanotube reinforced hierarchical composites: Effect of CNT distribution on shearing strength. *Composites, Part B* **2016**, *88*, 201−211.

(3) Li, R.; Lachman, N.; Florin, P.; Wagner, H. D.; Wardle, B. L. Hierarchical carbon nanotube carbon fiber unidirectional composites with preserved tensile and interfacial properties. *Compos. Sci. Technol.* **2015**, *117*, 139−145.

(4) An, F.; Lu, C.; Li, Y.; Guo, J.; Lu, X.; Lu, H.; He, S.; Yang, Y. Preparation and characterization of carbon nanotube-hybridized carbon fiber to reinforce epoxy composite. *Mater. Eng.* **2012**, *33*, 197−202.

(5) Zhao, M.; Meng, L.; Ma, L.; Ma, L.; Yang, X.; Huang, Y.; Ryu, J. E.; Shankar, A.; Li, T.; Yan, C.; Guo, Z. Layer-by-layer grafting CNTs onto carbon fibers surface for enhancing the interfacial properties of epoxy resin composites. *Compos. Sci. Technol.* **2018**, *154*, 28−36.

(6) Kalfon-Cohen, E.; Kopp, R.; Furtado, C.; Ni, X.; Arteiro, A.; Borstnar, G.; Mavrogordato, M. N.; Sinclair, I.; Spearing, S. M.; Camanho, P. P.; Wardle, B. L. Synergetic effects of thin plies and aligned carbon nanotube interlaminar reinforcement in composite laminates. *Compos. Sci. Technol.* **2018**, *166*, 160−168.

(7) Zhou, H.; Du, X.; Liu, H.-Y.; Zhou, H.; Zhang, Y.; Mai, Y.-W. J. C. S. Technology, Delamination toughening of carbon fiber/epoxy laminates by hierarchical carbon nanotube-short carbon fiber interleaves. *Compos. Sci. Technol.* **2017**, *140*, 46−53.

(8) White, K. L.; Sue, H.-J. J. P. Delamination toughness of fiber-reinforced composites containing a carbon nanotube/polyamide-12 epoxy thin film interlayer. *Polymer* **2012**, *53* (1), 37−42.

(9) Hawkins, S. A.; Yao, H.; Wang, H.; Sue, H.-J. Tensile properties and electrical conductivity of epoxy composite thin films containing zinc oxide quantum dots and multi-walled carbon nanotubes. *Carbon* **2017**, *115*, 18−27.

(10) Spitalsky, Z.; Tasis, D.; Papagelis, K.; Galiotis, C. Carbon nanotube−polymer composites: Chemistry, processing, mechanical and electrical properties. *Prog. Polym. Sci.* **2010**, *35* (3), 357−401.

(11) Han, Z.; Fina, A. Thermal conductivity of carbon nanotubes and their polymer nanocomposites: A review. *Prog. Polym. Sci.* **2011**, *36* (7), 914−944.

(12) Sui, X.; Shi, J.; Yao, H.; Xu, Z.; Chen, L.; Li, X.; Ma, M.; Kuang, L.; Fu, H.; Deng, H. Interfacial and fatigue-resistant synergetic enhancement of carbon fiber/epoxy hierarchical composites via an electrophoresis deposited carbon nanotube-toughened transition layer. *Composites, Part A* **2017**, *92*, 134−144.

(13) Fenner, J. S.; Daniel, I. M. Hybrid nanoreinforced carbon/epoxy composites for enhanced damage tolerance and fatigue life. *Composites, Part A* **2014**, *65*, 47−56.

(14) White, K. L.; Sue, H.-J. Delamination toughness of fiber-reinforced composites containing a carbon nanotube/polyamide-12 epoxy thin film interlayer. *Polymer* **2012**, *53* (1), 37−42.

(15) Zhou, H.; Du, X.; Liu, H.-Y.; Zhou, H.; Zhang, Y.; Mai, Y.-W. Delamination toughening of carbon fiber/epoxy laminates by hierarchical carbon nanotube-short carbon fiber interleaves. *Compos. Sci. Technol.* **2017**, *140*, 46−53.

(16) Hersam, M. C. Progress towards monodisperse single-walled carbon nanotubes. *Nat. Nanotechnol.* **2008**, *3*, 387.

(17) Punetha, V. D.; Rana, S.; Yoo, H. J.; Chaurasia, A.; McLeskey, J. T.; Ramasamy, M. S.; Sahoo, N. G.; Cho, J. W. Functionalization of carbon nanomaterials for advanced polymer nanocomposites: A comparison study between CNT and graphene. *Prog. Polym. Sci.* **2017**, *67*, 1−47.

(18) Fujigaya, T.; Nakashima, N. Non-covalent polymer wrapping of carbon nanotubes and the role of wrapped polymers as functional dispersants. *Sci. Technol. Adv. Mater.* **2015**, *16* (2), 024802.

(19) Bekyarova, E.; Thostenson, E. T.; Yu, A.; Kim, H.; Gao, J.; Tang, J.; Hahn, H. T.; Chou, T. W.; Itkis, M. E.; Haddon, R. C. Multiscale Carbon Nanotube-Carbon Fiber Reinforcement for Advanced Epoxy Composites. *Langmuir* **2007**, *23* (7), 3970−3974.

(20) Kamae, T.; Drzal, L. T. Carbon fiber/epoxy composite property enhancement through incorporation of carbon nanotubes at the fiber−matrix interphase − Part I: The development of carbon nanotube coated carbon fibers and the evaluation of their adhesion. *Composites, Part A* **2012**, *43* (9), 1569−1577.

(21) Peng, Q.; He, X.; Li, Y.; Wang, C.; Wang, R.; Hu, P.; Yan, Y.; Sritharan, T. Chemically and uniformly grafting carbon nanotubes onto carbon fibers by poly(amidoamine) for enhancing interfacial strength in carbon fiber composites. *J. Mater. Chem.* **2012**, *22* (13), 5928−5931.

(22) Park, S. K.; Mahmood, Q.; Park, H. S. Surface functional groups of carbon nanotubes to manipulate capacitive behaviors. *Nanoscale* **2013**, *5* (24), 12304−12309.

(23) Sankal, S.; Kaynak, C. Using various techniques to characterize oxidative functionalized and aminosilanized carbon nanotubes for polyamide matrix. *J. Reinf. Plast. Compos.* **2013**, *32* (2), 75−86.

(24) Kokkada, P.; Roy, S.; Lu, H. Carbon Nanotube Sheet Scrolled Fiber Composite for Enhanced Interfacial Mechanical Properties. *Proceedings of the American Society for Composites 2016: Thirty-First Technical Conference on Composite Materials*, September 19−22, 2016, Williamsburg, VA; DEStech Publications Inc., 2016.

(25) Guo, J.; Lu, C. Continuous preparation of multiscale reinforcement by electrophoretic deposition of carbon nanotubes onto carbon fiber tows. *Carbon* **2012**, *50* (8), 3101−3103.

(26) Yuan, X.; Zhu, B.; Cai, X.; Qiao, K.; Zhao, S.; Zhang, M.; Yu, J. Micro-configuration controlled interfacial adhesion by grafting graphene oxide onto carbon fibers. *Composites, Part A* **2018**, *111*, 83−93.

(27) Wilson, B. P.; Yliniemi, K.; Gestranius, M.; Hakalahti, M.; Putkonen, M.; Lundström, M.; Karppinen, M.; Tammelin, T.; Kontturi, E. Structural distinction due to deposition method in ultrathin films of cellulose nanofibres. *Cellulose* **2018**, *25* (3), 1715−1724.

(28) Awan, F. S.; Fakhar, M. A.; Khan, L. A.; Zaheer, U.; Khan, A. F.; Subhani, T. Interfacial mechanical properties of carbon nanotube-deposited carbon fiber epoxy matrix hierarchical composites. *Compos. Interfaces* **2018**, *25* (8), 681−699.

(29) Diba, M.; Fam, D. W. H.; Boccaccini, A. R.; Shaffer, M. S. P. Electrophoretic deposition of graphene-related materials: A review of the fundamentals. *Prog. Mater. Sci.* **2016**, *82*, 83−117.

(30) Wang, C.; Li, J.; Sun, S.; Li, X.; Zhao, F.; Jiang, B.; Huang, Y. Electrophoretic deposition of graphene oxide on continuous carbon fibers for reinforcement of both tensile and interfacial strength. *Compos. Sci. Technol.* **2016**, *135*, 46−53.

(31) Felisberto, M.; Tzounis, L.; Sacco, L.; Stamm, M.; Candal, R.; Rubiolo, G. H.; Goyanes, S. Carbon nanotubes grown on carbon fiber yarns by a low temperature CVD method: A significant enhancement of the interfacial adhesion between carbon fiber/epoxy matrix hierarchical composites. *Composites Communications* **2017**, *3*, 33−37.

(32) Zhang, H.; Liu, Y.; Kuwata, M.; Bilotti, E.; Peijs, T. Improved fracture toughness and integrated damage sensing capability by spray coated CNTs on carbon fibre prepreg. *Composites, Part A* **2015**, *70*, 102−110.

(33) Godara, A.; Gorbatikh, L.; Kalinka, G.; Warrier, A.; Rochez, O.; Mezzo, L.; Luizi, F.; van Vuure, A. W.; Lomov, S. V.; Verpoest, I. Interfacial shear strength of a glass fiber/epoxy bonding in composites modified with carbon nanotubes. *Compos. Sci. Technol.* **2010**, *70* (9), 1346−1352.

(34) Dong, L.; Hou, F.; Li, Y.; Wang, L.; Gao, H.; Tang, Y. Preparation of continuous carbon nanotube networks in carbon fiber/epoxy composite. *Composites, Part A* **2014**, *56*, 248−255.

(35) Qiu, J.; Zhang, C.; Wang, B.; Liang, R. Carbon nanotube integrated multifunctional multiscale composites. *Nanotechnology* **2007**, *18* (27), 275708.

https://dx.doi.org/10.1021/acsanm.0c00785
ACS Appl. Nano Mater. XXXX, XXX, XXX−XXX

(36) Pedrazzoli, D.; Pegoretti, A.; Kalaitzidou, K. Synergistic effect of exfoliated graphite nanoplatelets and short glass fiber on the mechanical and interfacial properties of epoxy composites. *Compos. Sci. Technol.* **2014**, *98*, 15−21.
(37) Sharma, M.; Gao, S.; Mäder, E.; Sharma, H.; Wei, L. Y.; Bijwe, J. Carbon fiber surfaces and composite interphases. *Compos. Sci. Technol.* **2014**, *102*, 35−50.
(38) Laachachi, A.; Vivet, A.; Nouet, G.; Ben Doudou, B.; Poilâne, C.; Chen, J.; Bo bai, J.; Ayachi, M. H. A chemical method to graft carbon nanotubes onto a carbon fiber. *Mater. Lett.* **2008**, *62* (3), 394−397.
(39) An, F.; Lu, C.; Guo, J.; He, S.; Lu, H.; Yang, Y. Preparation of vertically aligned carbon nanotube arrays grown onto carbon fiber fabric and evaluating its wettability on effect of composite. *Appl. Surf. Sci.* **2011**, *258* (3), 1069−1076.
(40) Deng, S. H.; Zhou, X. D.; Zhu, M. Q.; Fan, C. J.; Lin, Q. F. Interfacial toughening and consequent improvement in fracture toughness of carbon fiber reinforced epoxy resin composites: induced by diblock copolymers. *eXPRESS Polym. Lett.* **2013**, *7* (11), 925−935.
(41) Pramanik, C.; Gissinger, J. R.; Kumar, S.; Heinz, H. Carbon Nanotube Dispersion in Solvents and Polymer Solutions: Mechanisms, Assembly, and Preferences. *ACS Nano* **2017**, *11* (12), 12805−12816.
(42) Tamrakar, S.; An, Q.; Thostenson, E. T.; Rider, A. N.; Haque, B. Z.; Gillespie Jr, J. W. Tailoring interfacial properties by controlling carbon nanotube coating thickness on glass fibers using electrophoretic deposition. *ACS Appl. Mater. Interfaces* **2016**, *8* (2), 1501−1510.
(43) Vaisman, L.; Wagner, H. D.; Marom, G. The role of surfactants in dispersion of carbon nanotubes. *Adv. Colloid Interface Sci.* **2006**, *128*, 37−46.
(44) Ajayan, P. M.; Tour, J. M. Materials science: nanotube composites. *Nature* **2007**, *447* (7148), 1066.
(45) Sun, L.; Warren, G. L.; O'Reilly, J. Y.; Everett, W. N.; Lee, S. M.; Davis, D.; Lagoudas, D.; Sue, H. J. Mechanical properties of surface-functionalized SWCNT/epoxy composites. *Carbon* **2008**, *46* (2), 320−328.
(46) Gómez, S.; Rendtorff, N. M.; Aglietti, E. F.; Sakka, Y.; Suárez, G. J. A. S. S. Surface modification of multiwall carbon nanotubes by sulfonitric treatment. *Appl. Surf. Sci.* **2016**, *379*, 264−269.
(47) Moon, R. J.; Martini, A.; Nairn, J.; Simonsen, J.; Youngblood, J. Cellulose nanomaterials review: structure, properties and nanocomposites. *Chem. Soc. Rev.* **2011**, *40* (7), 3941−3994.
(48) Lee, K.-Y.; Aitomäki, Y.; Berglund, L. A.; Oksman, K.; Bismarck, A. On the use of nanocellulose as reinforcement in polymer matrix composites. *Compos. Sci. Technol.* **2014**, *105* (0), 15−27.
(49) Tang, L.; Weder, C. Cellulose Whisker/Epoxy Resin Nanocomposites. *ACS Appl. Mater. Interfaces* **2010**, *2* (4), 1073−1080.
(50) Chatterjee, S.; Nafezarefi, F.; Tai, N.; Schlagenhauf, L.; Nüesch, F.; Chu, B. Size and synergy effects of nanofiller hybrids including graphene nanoplatelets and carbon nanotubes in mechanical properties of epoxy composites. *Carbon* **2012**, *50* (15), 5380−5386.
(51) Yang, S.-Y.; Lin, W.-N.; Huang, Y.-L.; Tien, H.-W.; Wang, J.-Y.; Ma, C.-C. M.; Li, S.-M.; Wang, Y.-S. Synergetic effects of graphene platelets and carbon nanotubes on the mechanical and thermal properties of epoxy composites. *Carbon* **2011**, *49* (3), 793−803.
(52) Maiti, S.; Shrivastava, N. K.; Suin, S.; Khatua, B. Polystyrene/MWCNT/graphite nanoplate nanocomposites: efficient electromagnetic interference shielding material through graphite nanoplate−MWCNT−graphite nanoplate networking. *ACS Appl. Mater. Interfaces* **2013**, *5* (11), 4712−4724.
(53) Yu, A.; Ramesh, P.; Sun, X.; Bekyarova, E.; Itkis, M. E.; Haddon, R. C. Enhanced thermal conductivity in a hybrid graphite nanoplatelet−carbon nanotube filler for epoxy composites. *Adv. Mater.* **2008**, *20* (24), 4740−4744.
(54) Li, W.; Dichiara, A.; Bai, J. Carbon nanotube−graphene nanoplatelet hybrids as high-performance multifunctional reinforcements in epoxy composites. *Compos. Sci. Technol.* **2013**, *74*, 221−227.
(55) Sun, D.; Everett, W. N.; Chu, C. C.; Sue, H. J. Single□Walled Carbon□Nanotube Dispersion with Electrostatically Tethered Nanoplatelets. *Small* **2009**, *5* (23), 2692−2697.
(56) Sun, D.; Chu, C.-C.; Sue, H.-J. Simple approach for preparation of epoxy hybrid nanocomposites based on carbon nanotubes and a model clay. *Chem. Mater.* **2010**, *22* (12), 3773−3778.
(57) Nuruddin, M.; Gupta, R.; Tcherbi-Narteh, A.; Hosur, M.; Jeelani, S. Synergistic Effect of Graphene Nanoplatelets and Nanoclay on Epoxy Polymer Nanocomposites. *Adv. Mater. Res.* **2015**, *1119*, 155−159.
(58) Nuruddin, M.; Hosur, M.; Gupta, R.; Hosur, G.; Tcherbi-Narteh, A.; Jeelani, S. Cellulose Nanofibers-Graphene Nanoplatelets Hybrids Nanofillers as High-Performance Multifunctional Reinforcements in Epoxy Composites. *Polym. Polym. Compos.* **2017**, *25* (4), 273.
(59) Liu, P.; White, K. L.; Sugiyama, H.; Xi, J.; Higuchi, T.; Hoshino, T.; Ishige, R.; Jinnai, H.; Takahara, A.; Sue, H.-J. Influence of Trace Amount of Well-Dispersed Carbon Nanotubes on Structural Development and Tensile Properties of Polypropylene. *Macromolecules* **2013**, *46* (2), 463−473.
(60) Chu, C.-C.; White, K. L.; Liu, P.; Zhang, X.; Sue, H.-J. Electrical conductivity and thermal stability of polypropylene containing well-dispersed multi-walled carbon nanotubes disentangled with exfoliated nanoplatelets. *Carbon* **2012**, *50* (12), 4711−4721.
(61) Xin, F.; Li, L. Decoration of carbon nanotubes with silver nanoparticles for advanced CNT/polymer nanocomposites. *Composites, Part A* **2011**, *42* (8), 961−967.
(62) Nasirpouri, F.; Daneshvar-Fattah, F.; Samardak, A.; Sukovatitsina, E.; Ognev, A.; Chebotkevich, L. Magnetic Properties of Electrodeposited Nickel-Multiwall Carbon Nanotube Composite Films. *IEEE Trans. Magn.* **2015**, *51* (11), 1.
(63) Satishkumar, B. C.; Vogl, E. M.; Govindaraj, A.; Rao, C. N. R. The decoration of carbon nanotubes by metal nanoparticles. *J. Phys. D: Appl. Phys.* **1996**, *29* (12), 3173.
(64) Mougel, J.-B.; Adda, C.; Bertoncini, P.; Capron, I.; Cathala, B.; Chauvet, O. Highly Efficient and Predictable Noncovalent Dispersion of Single-Walled and Multi-Walled Carbon Nanotubes by Cellulose Nanocrystals. *J. Phys. Chem. C* **2016**, *120* (39), 22694−22701.
(65) Olivier, C.; Moreau, C. l.; Bertoncini, P.; Bizot, H.; Chauvet, O.; Cathala, B. Cellulose nanocrystal-assisted dispersion of luminescent single-walled carbon nanotubes for layer-by-layer assembled hybrid thin films. *Langmuir* **2012**, *28* (34), 12463−12471.
(66) Hamedi, M. M.; Hajian, A.; Fall, A. B.; Håkansson, K.; Salajkova, M.; Lundell, F.; Wågberg, L.; Berglund, L. A. Highly conducting, strong nanocomposites based on nanocellulose-assisted aqueous dispersions of single-wall carbon nanotubes. *ACS Nano* **2014**, *8* (3), 2467−2476.
(67) Liu, Y.; Sun, B.; Li, J.; Cheng, D.; An, X.; Yang, B.; He, Z.; Lutes, R.; Khan, A.; Ni, Y. Aqueous Dispersion of Carbon Fibers and Expanded Graphite Stabilized from the Addition of Cellulose Nanocrystals to Produce Highly Conductive Cellulose Composites. *ACS Sustainable Chem. Eng.* **2018**, *6* (3), 3291−3298.
(68) Sun, J.; Zhang, C.; Yuan, Z.; Ji, X.; Fu, Y.; Li, H.; Qin, M. Composite Films with Ordered Carbon Nanotubes and Cellulose Nanocrystals. *J. Phys. Chem. C* **2017**, *121* (16), 8976−8981.
(69) Carrasco, P. M.; Montes, S.; García, I.; Borghei, M.; Jiang, H.; Odriozola, I.; Cabañero, G.; Ruiz, V. High-concentration aqueous dispersions of graphene produced by exfoliation of graphite using cellulose nanocrystals. *Carbon* **2014**, *70*, 157−163.
(70) Wang, M.; Anoshkin, I. V.; Nasibulin, A. G.; Korhonen, J. T.; Seitsonen, J.; Pere, J.; Kauppinen, E. I.; Ras, R. H.; Ikkala, O. Modifying native nanocellulose aerogels with carbon nanotubes for mechanoresponsive conductivity and pressure sensing. *Adv. Mater.* **2013**, *25* (17), 2428−2432.
(71) Koga, H.; Saito, T.; Kitaoka, T.; Nogi, M.; Suganuma, K.; Isogai, A. Transparent, conductive, and printable composites consisting of TEMPO-oxidized nanocellulose and carbon nanotube. *Biomacromolecules* **2013**, *14* (4), 1160−1165.

https://dx.doi.org/10.1021/acsanm.0c00785
ACS Appl. Nano Mater. XXXX, XXX, XXX−XXX

(72) Hajian, A.; Lindström, S. B.; Pettersson, T. r.; Hamedi, M. M.; Wagberg, L. Understanding the dispersive action of nanocellulose for carbon nanomaterials. *Nano Lett.* **2017**, *17* (3), 1439−1447.
(73) Batmaz, R.; Mohammed, N.; Zaman, M.; Minhas, G.; Berry, R. M.; Tam, K. C. Cellulose nanocrystals as promising adsorbents for the removal of cationic dyes. *Cellulose* **2014**, *21* (3), 1655−1665.
(74) Huq, T.; Salmieri, S.; Khan, A.; Khan, R. A.; Le Tien, C.; Riedl, B.; Fraschini, C.; Bouchard, J.; Uribe-Calderon, J.; Kamal, M. R.; Lacroix, M. Nanocrystalline cellulose (NCC) reinforced alginate based biodegradable nanocomposite film. *Carbohydr. Polym.* **2012**, *90* (4), 1757−1763.
(75) Sun, B.; Hou, Q.; He, Z.; Liu, Z.; Ni, Y. Cellulose nanocrystals (CNC) as carriers for a spirooxazine dye and its effect on photochromic efficiency. *Carbohydr. Polym.* **2014**, *111*, 419−424.
(76) Wen, C.; Yuan, Q.; Liang, H.; Vriesekoop, F. Preparation and stabilization of d-limonene Pickering emulsions by cellulose nanocrystals. *Carbohydr. Polym.* **2014**, *112*, 695−700.
(77) Lin, N.; Dufresne, A. Surface chemistry, morphological analysis and properties of cellulose nanocrystals with gradiented sulfation degrees. *Nanoscale* **2014**, *6* (10), 5384−5393.
(78) Foster, E. J.; Moon, R. J.; Agarwal, U. P.; Bortner, M. J.; Bras, J.; Camarero-Espinosa, S.; Chan, K. J.; Clift, M. J.; Cranston, E. D.; Eichhorn, S. J.; et al. Current characterization methods for cellulose nanomaterials. *Chem. Soc. Rev.* **2018**, *47* (8), 2609−2679.
(79) Kharisov, B. I.; Kharissova, O. V.; Leija Gutierrez, H.; Ortiz Méndez, U. Recent advances on the soluble carbon nanotubes. *Ind. Eng. Chem. Res.* **2009**, *48* (2), 572−590.
(80) Ziegler, K. J.; Gu, Z.; Peng, H.; Flor, E. L.; Hauge, R. H.; Smalley, R. E. Controlled oxidative cutting of single-walled carbon nanotubes. *J. Am. Chem. Soc.* **2005**, *127* (5), 1541−1547.
(81) Ma, P. C.; Kim, J.-K.; Tang, B. Z. Effects of silane functionalization on the properties of carbon nanotube/epoxy nanocomposites. *Compos. Sci. Technol.* **2007**, *67* (14), 2965−2972.
(82) Olivier, C.; Moreau, C. l.; Bertoncini, P.; Bizot, H.; Chauvet, O.; Cathala, B. J. L. Cellulose nanocrystal-assisted dispersion of luminescent single-walled carbon nanotubes for layer-by-layer assembled hybrid thin films. *Langmuir* **2012**, *28* (34), 12463−12471.
(83) Mougel, J.-B.; Adda, C.; Bertoncini, P.; Capron, I.; Cathala, B.; Chauvet, O. Highly efficient and predictable noncovalent dispersion of single-walled and multi-walled carbon nanotubes by cellulose nanocrystals. *J. Phys. Chem. C* **2016**, *120* (39), 22694−22701.
(84) Zhao, F.; Huang, Y. J. J. o. M. C. Grafting of polyhedral oligomeric silsesquioxanes on a carbon fiber surface: novel coupling agents for fiber/polymer matrix composites. *J. Mater. Chem.* **2011**, *21* (11), 3695−3703.
(85) Chakraborty, A. K.; Plyhm, T.; Barbezat, M.; Necola, A.; Terrasi, G. P. Carbon nanotube (CNT)−epoxy nanocomposites: a systematic investigation of CNT dispersion. *J. Nanopart. Res.* **2011**, *13* (12), 6493−6506.
(86) Lesiak, B.; Kövér, L.; Tóth, J.; Zemek, J.; Jiricek, P.; Kromka, A.; Rangam, N. J. A. S. S. C sp2/sp3 hybridisations in carbon nanomaterials−XPS and (X) AES study. *Appl. Surf. Sci.* **2018**, *452*, 223−231.
(87) Tzounis, L.; Kirsten, M.; Simon, F.; Mäder, E.; Stamm, M. J. C. The interphase microstructure and electrical properties of glass fibers covalently and non-covalently bonded with multiwall carbon nanotubes. *Carbon* **2014**, *73*, 310−324.
(88) Yue, Z.; Jiang, W.; Wang, L.; Gardner, S.; Pittman, C. J. C. Surface characterization of electrochemically oxidized carbon fibers. *Carbon* **1999**, *37* (11), 1785−1796.
(89) Hashin, Z. Thermoelastic properties of fiber composites with imperfect interface. *Mech. Mater.* **1990**, *8* (4), 333−348.
(90) Nairn, J. A. J. A. C. L. Generalized shear-lag analysis including imperfect interfaces. *Advanced Composites Letters* **2004**, *13* (6), 096369350401300.
(91) Gao, S.-L.; Mäder, E. Characterisation of interphase nanoscale property variations in glass fibre reinforced polypropylene and epoxy resin composites. *Composites, Part A* **2002**, *33* (4), 559−576.
(92) Wernik, J. M.; Cornwell-Mott, B. J.; Meguid, S. A. Determination of the interfacial properties of carbon nanotube reinforced polymer composites using atomistic-based continuum model. *Int. J. Solids Struct.* **2012**, *49* (13), 1852−1863.
(93) Asadi, A.; Abusrea, M.; Arakawa, K.; Colton, J.; Kalaitzidou, K. E. P. L. I. p. A comparison of CFRP composite laminated joints fabricated with vacuum assisted resin transfer molding. *eXPRESS Polym. Lett.* **2018**, *12*, 781.
(94) Asadi, A.; Raghavan, J. Model for evolution of quasi-static transverse cracking in multiple plies of multidirectional polymer composite laminates. *Composite Structures* **2015**, *132*, 665−679.
(95) Asadi, A.; Miller, M.; Moon, R. J.; Kalaitzidou, K. Improving the interfacial and mechanical properties of short glass fiber/epoxy composites by coating the glass fibers with cellulose nanocrystals. *eXPRESS Polym. Lett.* **2016**, *10* (7), 587−597.
(96) Kaynan, O.; Atescan, Y.; Ozden-Yenigun, E.; Cebeci, H. J. C. P. B. E. Mixed Mode delamination in carbon nanotube/nanofiber interlayered composites. *Composites, Part B* **2018**, *154*, 186−194.
(97) Yuca, N.; Karatepe, N.; Yakuphanoglu, F. Thermal and electrical properties of carbon nanotubes purified by acid digestion. *World Acad. Sci. Eng. Technol.* **2011**, *79*, 611−616.
(98) Verma, P.; Saini, P.; Malik, R. S.; Choudhary, V. Excellent electromagnetic interference shielding and mechanical properties of high loading carbon-nanotubes/polymer composites designed using melt recirculation equipped twin-screw extruder. *Carbon* **2015**, *89*, 308−317.
(99) Wang, Z.-J.; Kwon, D.-J.; Choi, J.-Y.; Shin, P.-S.; Yi, J.-W.; Byun, J.-H.; Lee, H.-I.; Park, J.-K.; DeVries, K. L.; Park, J.-M. Inherent and interfacial evaluations of carbon nanotubes/epoxy composites and single carbon fiber at different temperatures. *Composites, Part B* **2016**, *91*, 111−118.
(100) Li, Z.; Lin, W.; Moon, K.-S.; Wilkins, S. J.; Yao, Y.; Watkins, K.; Morato, L.; Wong, C. Metal catalyst residues in carbon nanotubes decrease the thermal stability of carbon nanotube/silicone composites. *Carbon* **2011**, *49* (13), 4138−4148.
(101) Kashiwagi, T.; Grulke, E.; Hilding, J.; Harris, R.; Awad, W.; Douglas, J. Thermal Degradation and Flammability Properties of Poly(propylene)/Carbon Nanotube Composites. *Macromol. Rapid Commun.* **2002**, *23* (13), 761−765.

https://dx.doi.org/10.1021/acsanm.0c00785
ACS Appl. Nano Mater. XXXX, XXX, XXX−XXX